Extrusion-modulated DnaA activity oscillations coordinate DNA replication with biomass growth

Dengjin Li[1,2,6], Hai Zheng[1,2,6], Yang Bai[1,2,6], Zheng Zhang[1], Hao Cheng[1], Xiongliang Huang[1,2], Ting Wei[1], Matthew Wook Chang[3], Arieh Zaritsky[4], Terence Hwa[5], Chenli Liu[1,2,] ✉

[1]Key Laboratory of Quantitative Synthetic Biology, Shenzhen Institute of Synthetic Biology, Shenzhen Institutes of Advanced Technology, Chinese Academy of Sciences, Shenzhen 518055, China. [2]University of Chinese Academy of Sciences, Beijing 100049, China. [3]NUS Synthetic Biology for Clinical and Technological Innovation and Department of Biochemistry, Yong Loo Lin School of Medicine, National University of Singapore, Singapore; National Centre for Engineering Biology, Singapore. [4]Faculty of Natural Sciences, Ben-Gurion University of the Negev, Be'er Sheva, Israel. [5]Department of Physics & Department of Molecular Biology, University of California at San Diego, La Jolla, CA 92093-0319, USA. [6]These authors contributed equally: Dengjin Li, Hai Zheng, Yang Bai. ✉Email: cl.liu@siat.ac.cn

Abstract

Robust control of DNA replication is fundamental to bacterial proliferation. In *Escherichia coli*, replication initiation is thought to be regulated by oscillations in DnaA activity, driven by DnaA-chromosome interactions that differ among leading models. However, direct evidence linking these oscillations to replication initiation has been lacking, and existing models fail to explain the observed decoupling of replication initiation from *dnaA* expression. Here, we establish a direct link between DnaA activity and replication initiation by demonstrating robust oscillations in DnaA activity, which peak precisely at replication initiation across diverse growth conditions and genetic perturbations. Notably, these oscillations persist even when *dnaA* transcription remains constant, suggesting a regulatory mechanism that modulates DnaA activity independently of its expression. Additionally, we propose an extrusion model in which DNA-binding proteins sense biomass-DNA imbalance and extrude DnaA from the chromosome to trigger replication, overcoming limitations of existing models. Consistent with this model, perturbation of the nucleoid-associated protein H-NS modulates DnaA activity and replication timing, supporting its mechanistic validity.

Keywords: biomass-DNA coordination, chromosome replication initiation, DnaA activity oscillations, bacterial cell cycle

Introduction

Bacterial proliferation requires precise coordination between DNA replication and biomass growth to maintain cellular homeostasis. While biomass accumulates exponentially, DNA synthesis proceeds in a stepwise manner, creating temporal imbalances that demand continuous correction throughout the cell cycle (Fig. 1A-B). Failure to synchronize these processes risks catastrophic outcomes, such as growth defects, incomplete replication, unequal genetic segregation, and cell death (Boye et al., 1996; Khodursky et al., 2015; Lu et al., 1994; Mäkelä et al., 2024; Zaritsky & Pritchard, 1971). Central to this synchronization in *Escherichia coli* is the initiator protein DnaA, a DNA-binding protein that binds specifically to an asymmetric 9-bp DnaA-box, whose consensus sequence is TTWTNCACA (Hansen & Atlung, 2018; Speck et al., 1999). Although DnaA binding to the replication origin (*oriC*) triggers replication initiation (Dong et al., 2023; Kaguni, 2011; Ohbayashi et al., 2020; Ozaki & Katayama, 2012; Sekimizu et al., 1987), how DnaA activity—defined as the capacity to initiate replication—is dynamically regulated to coordinate DNA synthesis with cellular growth, particularly when DNA content and biomass diverge, remains a fundamental unresolved question in cell cycle biology.

Two competing models have dominated the field. The titration model posits that DnaA activity is governed by the availability of free DnaA, which accumulates until it surpasses the buffering capacity of chromosomal DnaA-boxes (Christensen et al., 1999; Hansen et al., 1991). Here, replication initiation resets the system by increasing DNA content (and thus DnaA-boxes), titrating excess DnaA. In contrast, the switch model emphasizes the ATP/ADP-bound states of DnaA: DnaA-ATP, synthesized during biomass growth, triggers initiation, while hydrolysis to DnaA-ADP following replication resets the cycle (Berger & Wolde, 2022; Donachie & Blakely, 2003; Fu et al., 2023; Hansen & Atlung, 2018; Katayama et al., 2017). Crucially, the titration model depends on ongoing DnaA synthesis to reflect biomass accumulation, whereas the switch model relies on nucleotide-state transitions, independent of total DnaA levels. Despite these mechanistic differences, both models consider that replication initiation is regulated by oscillations in DnaA activity, driven by DnaA-chromosome interactions (Fig. 1C). However, direct evidence linking these oscillations to replication initiation remains lacking. Moreover, neither model fully explains recent experimental observations: replication initiation persists for multiple generations even when *dnaA* transcription is completely inhibited (Knöppel et al., 2023). This discrepancy suggests an uncharacterized mechanism that senses biomass-DNA imbalance and directly modulates DnaA activity.

Here, using a synthetic reporter coupled with single-cell mRNA fluorescence *in situ* hybridization (FISH), we demonstrate that DnaA activity—governed by free DnaA concentration, DnaA-ATP/-ADP ratio, and orisome assembly competence—peaks precisely at initiation across diverse growth conditions and genetic backgrounds, even when *dnaA* transcription is held constant. DnaA activity oscillations persist independently of transcriptional feedback, pointing to a post-translational regulatory mechanism. We propose an extrusion model in which nucleoid-associated proteins (NAPs) sense biomass-DNA imbalance and dynamically extrude DnaA from the chromosome, liberating it to activate *oriC*. This model not only explains the decoupling of replication timing from *dnaA* expression but also integrates disparate experimental findings. Perturbations of the NAP, H-NS for instance, modulate DnaA activity and replication timing, directly supporting the model's predictions. By

unifying regulatory principles across transcription, protein activity, and chromosome dynamics, our findings advance the paradigm for bacterial replication control.

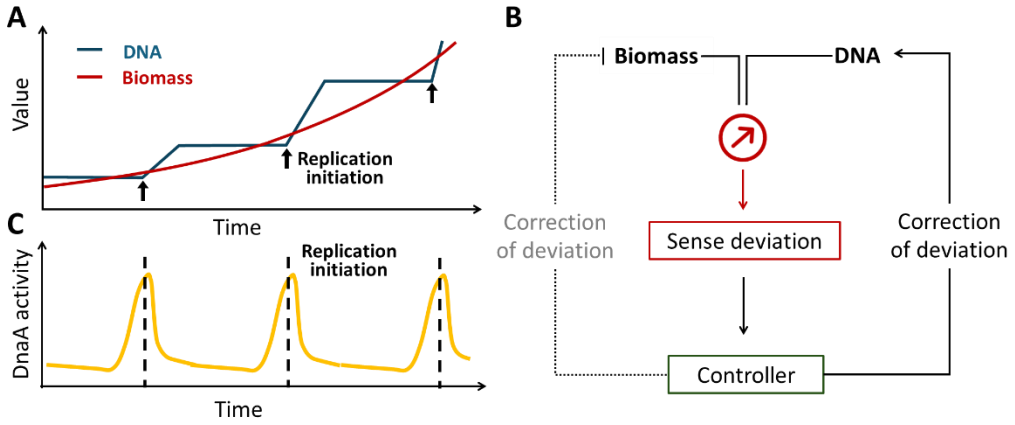

Figure 1. Coordination of biomass growth and DNA replication through replication initiation and DnaA activity oscillations. (A) Schematic representation of the discrepancy between biomass accumulation and DNA replication. While biomass grows exponentially, DNA synthesis progresses linearly, necessitating replication initiation events to maintain coordination. **(B)** Mechanistic model for biomass-DNA coordination in bacteria. A molecular sensor detects deviations between cell mass and DNA content, transmitting this information to regulatory controllers that compensate by either increasing DNA replication or restricting biomass accumulation. **(C)** Illustration of cyclic DnaA activity oscillations aligning with replication initiation to ensure precise cell cycle control.

Results

Development of a DnaA activity reporter system

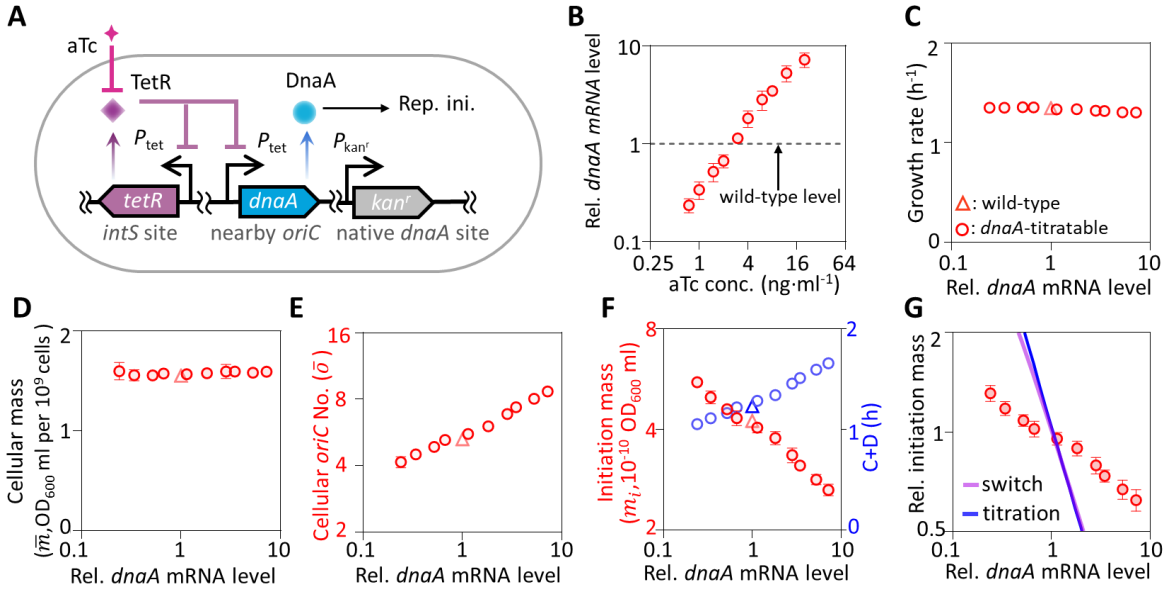

Figure 2. Construction and characterization of the *dnaA*-titratable strain. (A) Schematic of the *dnaA*-titratable strain. A *dnaA* gene under the control of the P_{tet} promoter was inserted near *oriC* and regulated by a P_{tet}-*tetR* feedback loop integrated at the *intS* locus, enabling fine-tuned expression control. The native *dnaA* gene was replaced with a kanamycin resistance cassette (*kan*^{r}). **(B–F)** Characterization of *dnaA*-titratable cells (circle) and wild-type MG1655 cells (triangle) grown in rich defined medium with glycerol (M6) under varying aTc concentrations. Measured parameters include: (**B**) *dnaA* mRNA levels; (**C**) growth rate; (**D**) population-averaged cellular mass; (**E**) population-averaged *oriC* numbers; (**F**) initiation mass (red, left axis) and the initiation to division period (C+D) (blue, right axis). The *dnaA* mRNA levels were normalized to that in wild-type cells. Cellular mass was determined by OD_{600} divided by cell number concentration. *oriC* copy numbers were measured using a run-out assay, and initiation mass was calculated as the ratio of cellular mass to *oriC* numbers. Data represent means ± SD (n = 5 biological replicates). **(G)** Relationship between relative initiation mass and relative *dnaA* mRNA levels, compared with predictions from the initiation titration model (blue line) and the switch model (purple line). The relative *dnaA* mRNA levels in experiments are compared to relative DnaA expression rate α_A in models. Experimental data are overlaid for validation.

It has been known that changing DnaA expression levels affects DnaA activity, and further changes initiation mass (Berger & Wolde, 2022; Løbner-Olesen et al., 1989; Zheng et al., 2020). To investigate this further, we engineered a *dnaA*-titratable strain, where *dnaA* transcription is controlled by an inducible P_{tet} promoter (Lutz & Bujard, 1997) (Fig. 2A). This system enabled precise modulation of *dnaA* mRNA levels (0.25 to 6 times the wild-type level) via anhydrotetracycline (aTc) induction (0.75–20 ng·ml^{-1}) without altering growth rate or cell size (Fig. 2B–D). As the DnaA expression level increases, DnaA activity reaches the initiation threshold earlier. Given that cell mass remained nearly unchanged, this earlier initiation led to an increase in population-averaged cellular *oriC* numbers (Fig. 2E). Concurrently, the initiation mass was reduced by 50%, and the period from initiation to division ($C + D$) was increased by ~60% (Fig. 2F). Notably, the observed relationship between DnaA

expression and initiation mass deviated significantly from both the titration and switch models (Fig. 2G; Supplementary Note S1), suggesting unaccounted regulatory mechanisms.

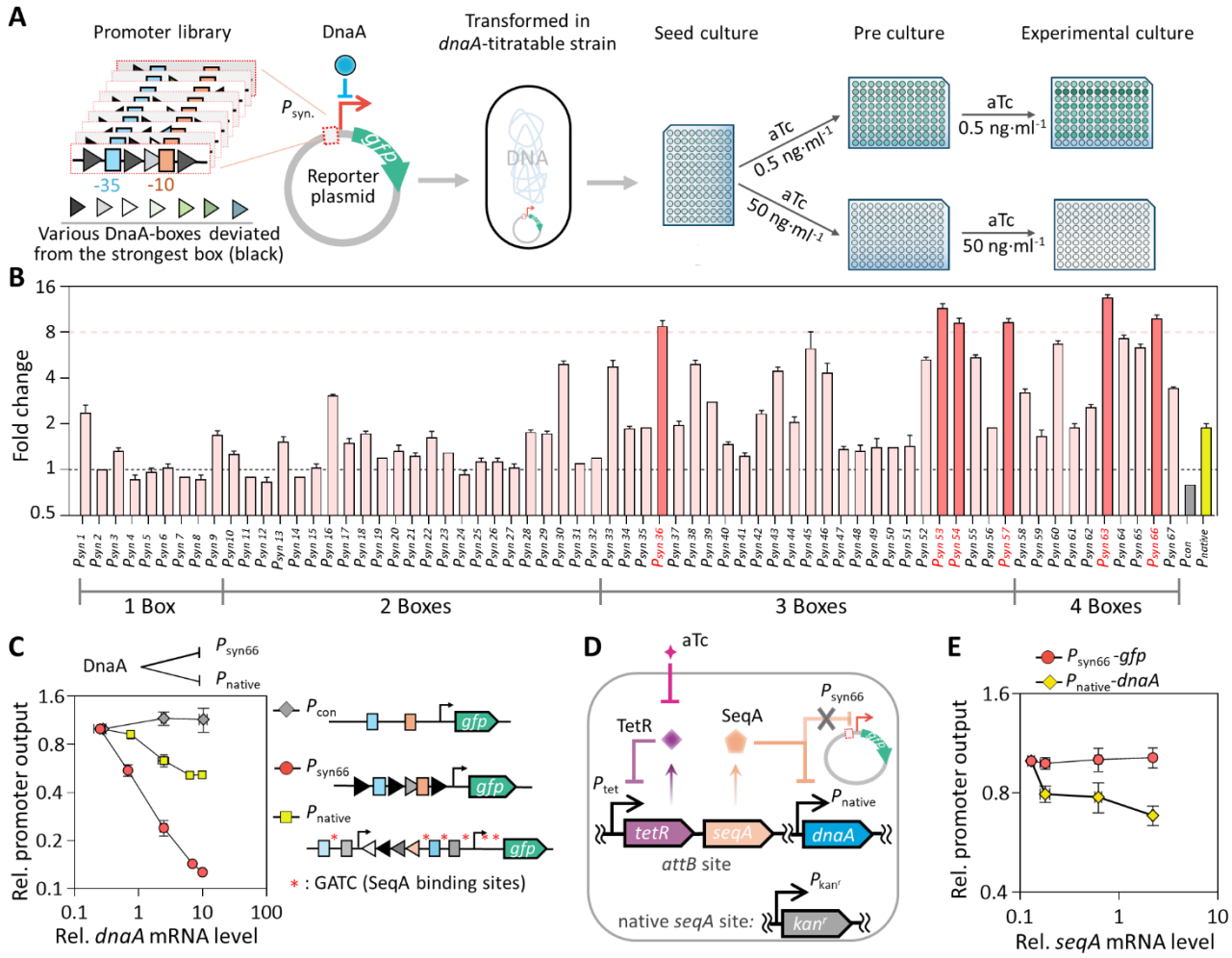

Figure 3. Development of a DnaA activity reporter system. (A) Schematic of promoter design and screening. Sixty-seven synthetic promoters were constructed by inserting various DnaA-boxes around the promoter core to drive *gfp* expression in a *dnaA*-titratable strain, where *dnaA* expression was regulated by aTc concentration. After pre-cultivation, GFP fluorescence per OD_{600} was measured using a microplate reader in cells grown under low (0.5 ng·ml^{-1}) or high (50 ng·ml^{-1}) aTc concentrations to determine repression fold-change. **(B)** Repression fold-change of synthetic promoters. P_{con} (a promoter lacking DnaA-boxes) and P_{native} (the endogenous *dnaA* promoter) served as negative and positive controls, shown in gray and yellow, respectively. **(C)** Response curves of three promoters to varying *dnaA* expression levels, with their promoter architectures shown on the right. Promoter activity was assessed by relative *gfp* mRNA levels, normalized to the lowest *dnaA* expression condition. Schematic **(D)** and response curves **(E)** of P_{syn66} and P_{native} responses to SeqA in the *seqA*-titratable strain. Promoter activity was quantified from *gfp* transcript levels in *seqA*-titratable cells containing the P_{syn66}-GFP plasmid, normalized to the lowest *seqA* expression level. All cells were grown in rich defined medium supplemented with glycerol across different aTc concentrations. Data represent mean ± SD from 3 biological replicates (**B**,**C**,**E**).

To dissect DnaA activity dynamics, we constructed a library of synthetic promoters (n = 67) by replacing *tetO* operators in P_{tet} with DnaA-boxes (Fig. S1). To assess the degree of DnaA activity-mediated repression, we measured the fold change in GFP expression driven by each synthetic promoter under low and high levels of *dnaA* induction (Fig. 3A). Six synthetic promoters exhibited over 8-fold DnaA-mediated repression, whereas the promoter lacking DnaA-boxes (P_{con}) showed none, and the well-characterized native *dnaA* promoter (P_{native})(Braun et al., 1985; Saggioro et al., 2013; Speck et al., 1999) displayed approximately two-fold repression (Fig. 3B; Fig. S1). P_{syn66}, which contains three strong and one weak DnaA-box, exhibited >8-fold repression under high DnaA induction (Fig. 3B). P_{syn66}'s design enables responsiveness to both free DnaA levels (via strong boxes) and the DnaA-ATP/DnaA-ADP ratio (via differential binding to the weak box)(Grimwade & Leonard, 2021; Katayama et al., 2017; Speck et al., 1999). Dose-response assays confirmed that P_{syn66} was progressively repressed across a 40-fold range of *dnaA* expression (Fig. 3C), with no interference from SeqA-mediated sequestration (Fig. 3D-E). These results validated P_{syn66} as a sensitive and specific reporter for DnaA activity.

Decoupling DnaA activity oscillations from *dnaA* transcription fluctuations

To investigate DnaA activity dynamics throughout the cell cycle, we linked P_{syn66} activity to cell size, a surrogate for cell-cycle progression, using single-cell mRNA FISH(Skinner et al., 2013) to quantify *lacZ* mRNA levels in MG1655*Δlac* cells harboring the P_{syn66}-*lacZ* plasmid (Fig. 4A). A control strain harboring a promoter-less *lacZ* construct (P_{neg}) showed undetectable fluorescence signals (Fig. 4A), confirming the specificity of *lacZ* mRNA detection. Quantitative analysis revealed that P_{syn66}-driven mRNA levels fluctuated approximately 3-fold over the cell cycle, whereas the DnaA-unresponsive constitutive promoter (P_{con}) exhibited stable expression (Fig. 4B). However, fluctuations in mRNA concentration may not directly correspond to changes in DnaA activity due to global factors such as plasmid copy number and RNA polymerase concentration (Balakrishnan et al., 2022; Bintu et al., 2005a; Bintu et al., 2005b). To account for these variables, we used a P_{con}-*lacZ* plasmid to estimate global effects on mRNA concentration and calculated DnaA activity by assuming that it is inversely proportional to $k_{syn66} = \frac{[mZ](\mathrm{P_{syn66}})}{[mZ](\mathrm{P_{con}})}$. In wild-type cells (MG1655*Δlac*) harboring the synthetic reporter system (Fig. 4C), fluctuations in DnaA activity, as denoted by k_{syn66}^{-1}, displayed approximately a 3-fold variation across the cell cycle (Fig. 4D), underscoring the substantial cell cycle-dependent oscillations in DnaA activity.

We then examined whether the observed fluctuations in DnaA activity were linked to oscillations in *dnaA* transcription. Comparing the dynamics of *dnaA* mRNA and DnaA activity, we found that the peak in DnaA activity coincided with the trough in *dnaA* mRNA levels (dashed line in Fig. 4D-E). To test whether *dnaA* transcription drives these oscillations, we eliminated transcriptional fluctuations using the *dnaA*-titratable strain. Despite constant *dnaA* mRNA levels (2 ng·ml^{-1} aTc induction), DnaA activity was retained consistent oscillations (Fig. 4F–H), demonstrating the decoupling of DnaA activity oscillations from transcriptional fluctuations. Our data suggest that post-translational regulation, not transcriptional feedback, governs the DnaA activity.

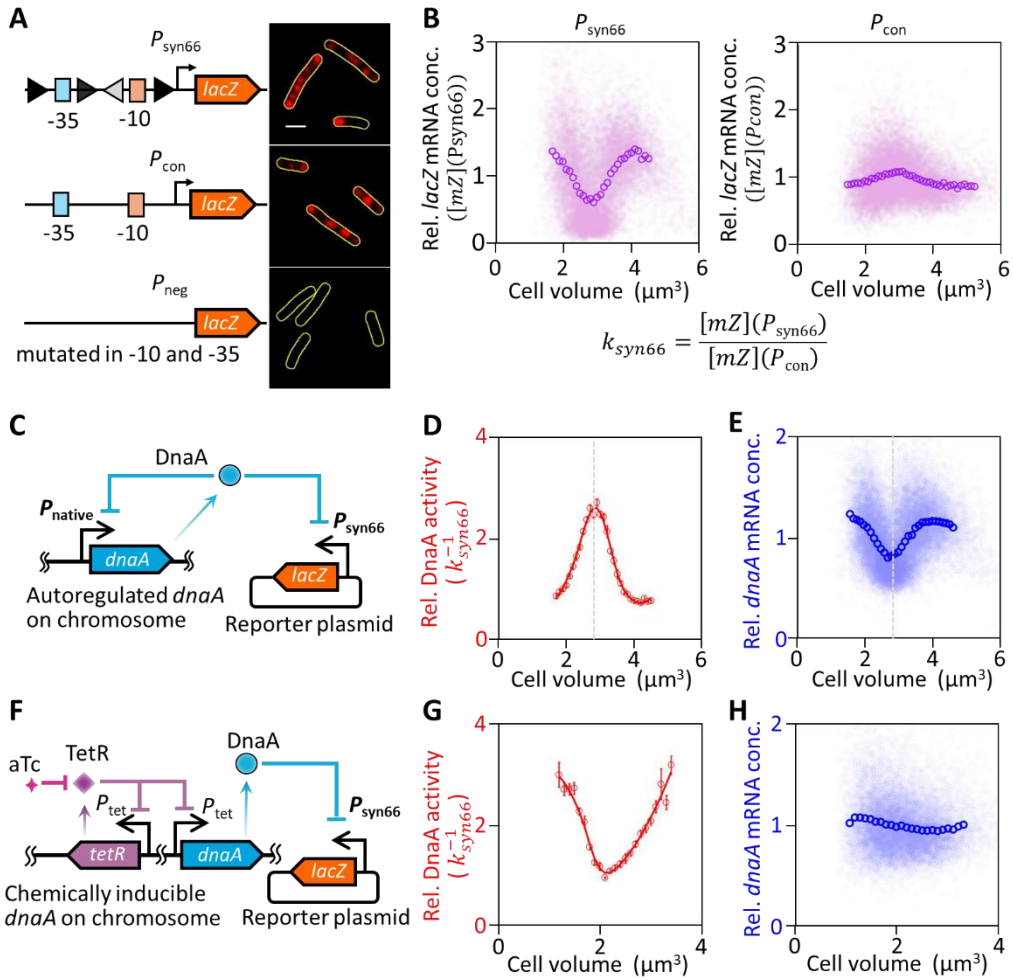

Figure 4. DnaA activity oscillations decoupled from *dnaA* transcription fluctuations. **(A)** Representative *lacZ* mRNA FISH images of MG1655 Δ*lac* cells transformed with *lacZ* expression plasmids driven by P_{syn66} (DnaA-boxes around promoter core), P_{con} (no DnaA-box around promoter core), or P_{neg} (mutated promoter core). Yellow outlines indicate cell boundaries identified from phase-contrast images. **(B)** Relative *lacZ* mRNA concentrations driven by P_{syn66} (left) and P_{con} (right) across different cell volumes. Relative concentrations were determined from volume-specific *lacZ* mRNA fluorescence intensities, normalized to the population average. Volume-binned data for P_{syn66} ($[mZ](P_{syn66})$) and P_{con} ($[mZ](P_{con})$) are shown as open circles and were used to calculate k_{syn66}. **(C)** Schematic of a strain with autoregulated *dnaA* transcription carrying a DnaA activity reporter plasmid. Cell cycle-dependent fluctuations in relative DnaA activity (**D**) and relative *dnaA* mRNA concentrations (**E**) in cells from panel **C**, grown in rich defined medium supplemented with glucose. Relative DnaA activity (k_{syn66}^{-1}), calculated from volume-binned data in panel **B**, was smoothed and plotted as a red curve (**D**). Relative *dnaA* mRNA concentrations were determined from volume-specific *dnaA* mRNA fluorescence intensities, normalized to the population average, with volume-binned data shown as open circles (**E**). Dashed lines indicate the cell volume at peak DnaA activity (**D**) and the minimum *dnaA* mRNA content (**E**). **(F–H)** Same as panels **C–E**, but for cells with aTc induced *dnaA* transcription, grown in rich defined medium supplemented with glycerol under 2 ng·ml^{-1} aTc induction. More than 8,000 cells were analyzed per growth condition, and all error bars correspond to standard error of the mean (SEM).

DnaA activity oscillations are tightly coupled to replication timing

To explore the relationship between DnaA activity oscillations and DNA replication initiation, we examined cells grown under various nutrient conditions supporting different doubling times (30–66 min). Significant fluctuations in DnaA activity were observed across all conditions (Fig. 5A). We also estimated the cell volume at replication initiation (V_i) based on population-averaged cell volume and *oriC* number (Bremer et al., 1979; Si et al., 2017; Zheng et al., 2016) (Fig. S2 A–C), marking this on the DnaA activity profiles. In a representative birth-to-division cell cycle (Pountain et al., 2024) (Fig. S2D), DnaA activity peaks consistently coincided with V_i, indicating a close correlation between DnaA activity and replication initiation (Fig. 5A).

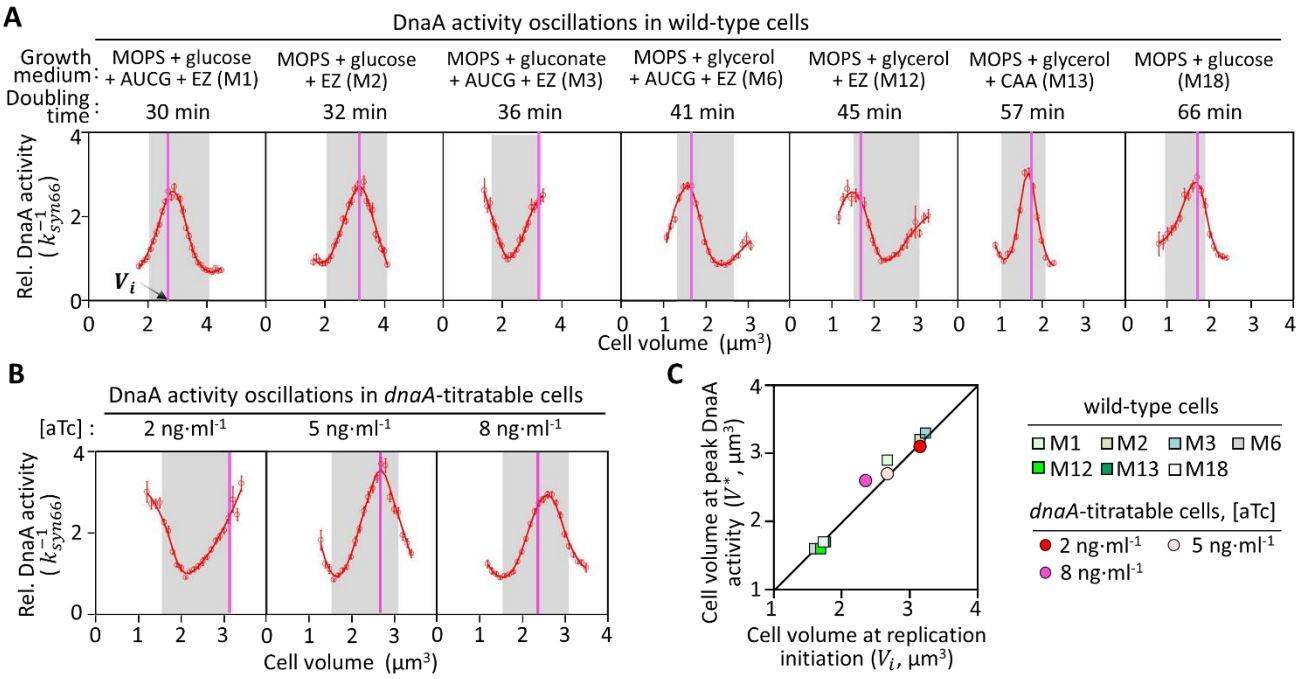

Figure 5. Tight correlation between DnaA activity oscillations and DNA replication initiation. (A) Cell cycle-dependent DnaA activity oscillations in wild-type cells across various growth conditions. DnaA activity is represented by k_{syn66}^{-1}. Volume-binned DnaA activity (red circles) was smoothed and plotted as a red curve. The representative birth-to-division cell cycle, defined as the cell volume doubling interval containing the majority of cells, is shaded in gray. The vertical line indicates the cell volume at replication initiation (V_i). **(B)** Cell cycle-dependent DnaA activity oscillations in *dnaA*-titratable cells grown in M6 medium with varying aTc concentrations. More than 8,000 cells were analyzed per growth condition, and error bars show the mean ± SEM. **(C)** Correlation between V^* and V_i in wild-type (squares) and *dnaA*-titratable (circles) cells. V^* represents the cell volume at the peak of DnaA activity within the representative birth-to-division cell cycle. The black line indicates equivalence between V^* and V_i.

Further genetic perturbations, such as titrating DnaA expression, shifted DnaA activity fluctuations, yet the relationship between V^* (the cell volume at maximal DnaA activity in a representative birth-to-division cell cycle) and V_i remained locked (Fig. 5B). To quantify this relationship, we compared V_i with V^*, revealing a strictly proportional relationship through the origin (slope= 1.0, R^2 = 0.98), indicating equivalence between V^* and V_i (Fig. 5C). These results confirm that DnaA activity oscillations are tightly correlated with replication initiation, independent of transcriptional or nutrient perturbations.

An extrusion model reconciles paradoxical initiation events

Very recently, Knöppel *et al.* reported that multiple rounds of initiation occurred even after DnaA synthesis is shut down (Knöppel et al., 2023). In their experiment, DnaA was supplied in excess before expression ceased (Knöppel et al., 2023), potentially allowing continued replication initiation due to residual DnaA. To address this issue, we shut down DnaA expression from its native level using the deactivated miniature Un1Cas12f1 (dUn1Cas12f1) system, guided by sgRNA to repress *dnaA* transcription (Fig. 6A). This system effectively diminished *dnaA* transcription to an extremely low level, yet total *oriC* numbers increased fourfold within 90 min, consistent with two rounds of replication initiation (Fig. 6B). These findings demonstrate that halting DnaA synthesis does not immediately abolish replication initiation.

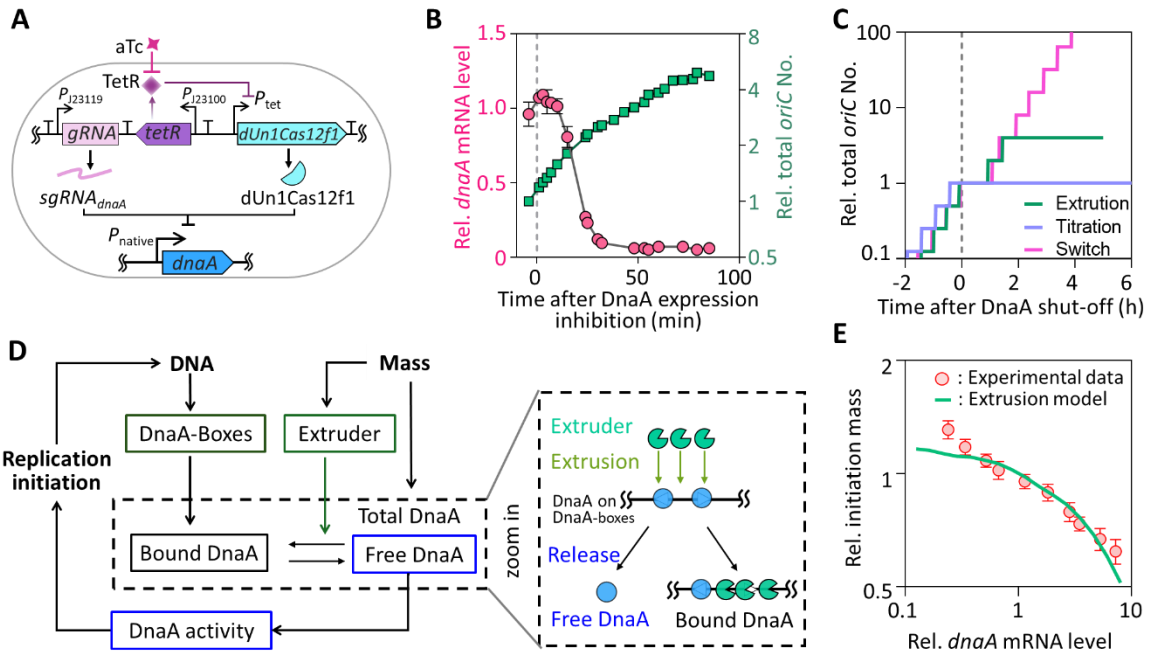

Figure 6. An extrusion model explains DnaA shut-down dynamics. (A) Genetic circuit of the deactivated CRISPR-Cas system for *dnaA* transcription shut-down. *dnaA* gene is targeted by a constitutively expressed sgRNA, while dUn1Cas12f1 expression is inhibited by TetR repressor. These transcription units are separated by terminators. The cassette was integrated into the chromosome near the *oriC* locus. DnaA shutdown is induced by the addition of aTc. **(B)** Time-course of relative *dnaA* mRNA levels (red line, left axis) and total *oriC* number (green line, right axis) following the addition of 50 ng·ml^{-1} aTc at time 0 (dashed line). *dnaA* mRNA levels were normalized to wild-type levels, and *oriC* numbers were normalized to their initial values. Error bars indicate mean ± SD (n = 3 biologically independent experiments). **(C)** Predicted increases in total *oriC* number during *dnaA* transcription shut-down based on three models: the titration model, switch model, and extrusion model. Shutdown was simulated by setting *dnaA* transcription to zero at time 0 (dashed line). **(D)** Schematic of the extrusion model. The model introduces extruder(s) as additional regulators of biomass-DNA coordination, complementing the role of DnaA (left). Increased binding of the extruder to DNA promotes the release of DnaA from DnaA-boxes (right). **(E)** Comparison of the relationship between relative initiation mass and relative *dnaA* mRNA levels from experimental data (Fig. 2F) and predictions of the extrusion model.

Both the titration and switch models predict a close relationship between DnaA activity oscillations and replication initiation(Berger & Wolde, 2022). However, they fail to account for the multiple rounds of initiation observed after DnaA synthesis was shut down. According to the titration model, initiation should cease immediately once DnaA expression is shut down, as the reduction in DnaA concentration would prevent it from reaching the threshold required to trigger new rounds of replication. In contrast, the switch model predicts infinite initiations following the cessation of DnaA expression (Fig. 6C). This is because the cessation of DnaA synthesis only reduce the production rate of DnaA-ATP and had no effect on the conversion rates between DnaA-ATP and DnaA-ADP. As a result, the ratio of DnaA-ATP to DnaA-ADP would temporarily decrease, causing a brief lag before initiation resumes indefinitely (Fig. 6C).

The failure of both models prompts us to revisit the regulatory mechanisms of replication initiation. In the titration model, a substantial fraction of DnaA proteins binds to DnaA-boxes along the chromosome, raising the possibility that these bound proteins serve as a reservoir of free DnaA, sustaining replication initiation even after DnaA synthesis ceases. We thus considered the possibility of some extruder(s) alongside DnaA to sense biomass-DNA deviation, and flush DnaA proteins away from the DnaA-boxes, thus releasing free DnaA to dynamically restore DnaA activity, even in the absence of ongoing DnaA synthesis (Fig. 6D).

In this proposed "extrusion model", the extruder is constitutively expressed, synthesized at a constant rate throughout the cell cycle, accumulating in proportion to biomass growth, enabling replication initiation when free DnaA concentrations exceed the critical threshold, as described in the titration model(Hansen & Atlung, 2018; Hansen et al., 1991) (Fig. 6D). This model guarantees the long-term coordination of biomass growth and *oriC* abundance, as well as stable oscillations in free DnaA and *oriC* concentrations (Fig. S3 A). Notably, the extrusion model accounts for the persistence of replication initiation and free DnaA oscillations over multiple cell cycles after DnaA synthesis is halted (Fig. 6C; Fig. S3 B). Moreover, since the extruder mitigates the impact of perturbations on DnaA synthesis, the model predicts a quantitative relationship between initiation mass and DnaA expression levels that aligns with experimental observations (Fig. 6E; Supplementary Note S1). Furthermore, a stochastic implementation of the extrusion model shows the lack of correlation between successive replication initiation events (Fig. S3 C), as observed in recent studies (Si et al., 2019; Witz et al., 2019).

Perturbation of H-NS validates the extrusion mechanism

The extrusion model could be validated by changing the expression level of the extruder, which modulates DnaA activity by releasing DnaA from DnaA-boxes. Given their DNA binding properties, NAPs(Dillon & Dorman, 2010) are likely candidates for this extruder role. Therefore, we selected H-NS(Dorman, 2004), a major NAP, which is capable of promoting the release of DnaA from bound DnaA-boxes *in vitro* (Fig. S4), to experimentally assess the validity of the extrusion model. To this end, we constructed a *hns*-titratable strain, incorporating a reporting plasmid to capture changes in DnaA activity across various H-NS expression levels (Fig. 7A). Under steady-state cultivation, increasing aTc concentrations from 0 to 50 $ng{\cdot}ml^{-1}$ resulted in *hns* mRNA levels ranging from 0.25 to 5 times the wild-type levels, without affecting growth rate (Fig. S5 A-B). Within this range, DnaA activity increased by approximately 60 % (Fig. 7B), while the initiation mass decreased by 30 % (Fig. 7C; calculated with Fig. 5S C-D), in qualitative agreement with the predictions of the extrusion model (Fig. S5 E-F).

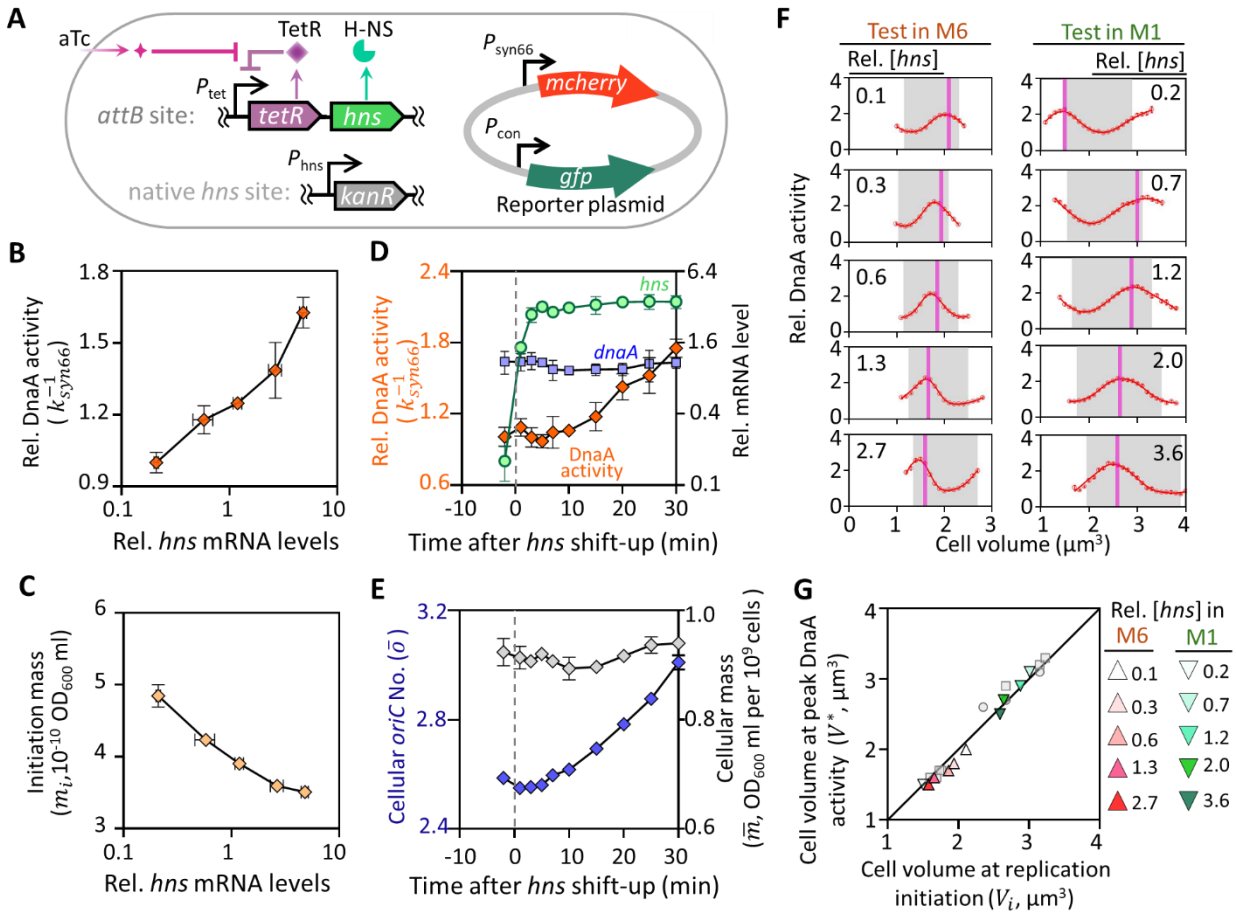

Figure 7. Titration of *hns* expression modulates DnaA activity and replication initiation. (A) Genetic circuit of the *hns*-titratable strain. Expression of *hns* is controlled by a P_{tet}-*tetR* negative feedback loop integrated at the *attB* site, with the native *hns* coding sequence replaced by a kanamycin resistance gene. The plasmid contains P_{syn66}-*mcherry* and P_{con}-*gfp* expression cassettes was used to assess DnaA activity. DnaA activity (**B**) and initiation mass (**C**) were characterized in M6 medium with varying *hns* expression levels during steady-state cultivation. **(D)** mRNA levels of *hns* (green circles) and *dnaA* (blue squares) relative to wild-type levels, along with DnaA activity (orange rhombus), were measured during *hns* shift-up. *hns* shift-up was induced by the addition of 50 ng·ml^{-1} aTc at time 0 (dashed line), following steady-state cultivation in M6 medium without aTc. **(E)** Dynamics of population-averaged *oriC* number (blue rhombus, left axis) and cellular mass (gray rhombus, right axis) during *hns* shift-up. Data represent mean ± SD from 3 biological replicates (**B-E**). **(F)** Cell cycle-dependent DnaA activity oscillations in *hns*-titratable cells cultivated in M1 and M6 media under varying aTc concentrations. Relative *hns* mRNA levels are indicated for each condition. More than 8,000 cells were analyzed for each condition and error bars show the mean ± SEM. **(G)** Correlation between the volume at maximal DnaA activity (V^*) and the volume at replication initiation (V_i) for *hns*-titratable cells grown in M1 (green down-pointing triangle) and M6 (red up-pointing triangle) media with varying *hns* expression levels. Data for *dnaA*-titratable cells (gray circles) and wild-type *dnaA*-autoregulated cells (Fig. 5C) are included for comparison.

Since H-NS is a global transcriptional regulator (Hommais et al., 2001), we wonder whether its effect on DnaA activity was mediated through *dnaA* transcription. To test this, we measured DnaA activity and *dnaA* mRNA levels during an H-NS shift-up. Upon addition of 50 ng·ml^{-1} aTc, *hns* levels increased

301 more than 20-fold within a short period, followed by approximately 80 % increase in DnaA activity,
302 with no significant change in *dnaA* mRNA levels (Fig. 7D). Additionally, cellular *oriC* content increased
303 significantly within 30 minutes, while cell mass remained unchanged (Fig. 7E). These results suggest
304 that the rapid increase in DnaA activity and accelerated replication initiation induced by H-NS
305 upregulation is not driven by changes in *dnaA* transcription.

306 Leveraging the *hns*-titratable strain, we re-examined the tight correlation between DnaA activity
307 oscillations and replication initiation. In two different growth media with varying *hns* levels, the peak
308 of DnaA activity fluctuations (V^*) shifted in concert with the independently measured volume at
309 replication initiation (V_i) (Fig. 7F). Plotting V^* against V_i, revealed the same equivalency observed
310 in wild-type and *dnaA*-titratable cells (Fig. 7G). Collectively, these results support the notion that
311 DnaA activity oscillations, modulated by extrusion, coordinate DNA replication and biomass growth.

312 Discussion

313 In this study, we proposed chromosome-driven DnaA activity oscillations as a post-translational
314 "rheostat" coordinating DNA replication with biomass growth in *E. coli*. By developing a SeqA-
315 independent synthetic promoter reporter (P_{syn66}) on a plasmid, we circumvented confounding factors
316 inherent to native systems (Pountain et al., 2024), thereby achieving the direct quantification of DnaA
317 activity dynamics. Crucially, these oscillations persist when *dnaA* transcription is fixed, operate
318 independently of SeqA-mediated repression, and peak precisely at replication initiation across all
319 tested growth conditions. This reveals an essential paradigm: bacteria bypass transcriptional control
320 to synchronize genome duplication with growth through regulation of DnaA-chromosome
321 interactions.

322 Very recently, Iuliani *et al.* also reported DnaA activity oscillations (Iuliani et al., 2024), which is a
323 significant milestone, innovatively using a chromosomal promoter reporter system and microfluidics
324 for single-cell DnaA activity observations. They revealed key relationships between DnaA activity, cell
325 size, and division. Our work, however, differs in multiple ways. Methodologically, we engineered a
326 *dnaA*-titratable strain and synthetic promoters like P_{syn66}, enabling precise *dnaA* expression control
327 and cleaner DnaA activity reporting. Our mRNA FISH approach uniquely compares DnaA activity and
328 transcription at the single-cell level. Replication initiation volume scales proportionally with peak
329 DnaA activity volume with a slope of 1.0 (R^2=0.98, Fig. 7G), indicating predictive correspondence
330 rather than absolute coincidence. While population-level V_i estimation cannot resolve single-cell
331 stochasticity, the consistent V^*:V_i relationship across 20 conditions suggests DnaA activity
332 thresholds predict initiation timing within physiological error margins. Regarding research questions,
333 while Iuliani *et al.* focused on DnaA-cell size-division relationships, we addressed the decoupling of
334 replication initiation from *dnaA* expression with our novel extrusion model.

335 Recently, an integrated "titration-switch" model has been proposed to improve replication cycle
336 stability across different growth rates (Berger & Wolde, 2022; Fu et al., 2023). Although this
337 integrated model predicts a relationship between initiation mass and *dnaA* mRNA levels that aligns
338 closely with steady-state experimental data (Fig. S6 A), it fails to account for the additional replication
339 initiation observed after *dnaA* shutdown (Fig. S6 B). By incorporating an extruder into this model, we
340 successfully reproduced the additional replication initiation (Fig. S6 C), thus validating the extrusion

concept and aligning with experimental observations. These findings highlight the critical role of extrusion in refining our mechanistic understanding of biomass-DNA coordination.

Mechanistically, we propose that NAPs sense biomass-DNA imbalances and extrude DnaA from chromosomal sites, converting physical displacement into biochemical activation, a spatial control strategy mirroring eukaryotic chromatin regulation. H-NS emerges as a prime extruder candidate given its DNA-condensing ability (Dame et al., 2000; Zimmerman, 2006) and replication-timing effects (Fig. 7). This functional multiplicity likely enhances robustness, allowing cells to maintain replication homeostasis despite fluctuating environments, an evolutionary advantage paralleling eukaryotic checkpoint system.

These findings refine bacterial cell cycle control as a dynamic interplay between physical chromosome remodeling and metabolic sensing. By tethering DnaA activation to biomass accumulation through extrusion, cells achieve an important capability: noise suppression via spatial filtering of transcriptional fluctuations. Such mechanistic parsimony, using chromosome structure to both store genetic information and regulate replication timing, may represent a potential organizational strategy. Indeed, parallels to eukaryotic systems are striking: DnaA extrusion resembles ORC licensing through chromatin accessibility (Fragkos et al., 2015), while biomass-DNA coupling evokes yeast size-control checkpoints (Xie et al., 2022).

While H-NS perturbation supports extrusion mechanism, future work should identify the full extruder interactome and elucidate how metabolic signals modulate their activity. Our synthetic reporter system provides a valuable tool for dissecting the spatial regulation of DNA-binding proteins, with translational potential in antimicrobial development (targeting pathogen-specific extruders) and synthetic biology (engineering tunable replication circuits). More broadly, this work establishes physical chromosome remodeling as a central coordinator of cellular homeostasis, a concept bridging prokaryotic and eukaryotic cell cycle paradigms.

Materials and Methods

Plasmid and strain Construction

Strains used in this study were derived from *E. coli* MG1655. Information for all strains and plasmids are listed in Tables S1 and S2.

Plasmids for reporting DnaA activity

Plasmids expressing GFP, mCherry, or LacZ under synthetic promoters were constructed based on the pPT plasmid backbone (Zong et al., 2017). The *lacZ* amplified from the MG1655 genome and mcherry gene amplified from pMD19-*hupA-mcherry* plasmid, were assembled into the BspQI/BsrGI-digested pPT backbone via the One Step Cloning Kit (Vazyme, C112), to generate the pPT-lacZ and pPT-RFP plasmids, respectively. Synthetic promoters, generated by annealing the primer pairs listed in Table S3, were ligated directly into the BsaI-digested pPT, pPT-RFP or pPT-lacZ plasmid as required. The native *dnaA* promoter (P_{native}) amplified from the MG1655 genome was digested with Bsa*I*, and ligated into the BsaI-digested pPT plasmid. The P_{con}-*gfp* cassette amplified from P_{con}-GFP plasmid was assembled into the SpeI-digested P_{syn66}-RFP plasmid to generate the P_{sny66}-P_{con}-FPs plasmid. Primer information for amplifying DNA fragments is detailed in Table S4.

Plasmids for strain construction

For constructing the plasmid pMD19-Rhns, pMD19-RseqA and pMD19-RdnaA, the *hns*, *seqA* and *dnaA* gene were amplified from MG1655 genome, digested, and ligated into the same enzyme-digested pMD19-tetR plasmid. For constructing the plasmid p15A-RdnaA, the T3-P_{tet}-*tetR-dnaA* cassette, *kan*^{r} gene and p15A-T1 fragment were amplified from plasmid pMD19-RdnaA, pEcCas and PZA31-P_{tet}-M2-GFP, respectively, and then assembled via MultiS One Step Cloning Kit (Vazyme, C113). The plasmid P_CRidnaA1 were obtained by ligating the annealed primer pairs to the BsaI-digested CPP00458 plasmid for the *dnaA* targeting. The chloramphenicol resistance gene *Cm*^{r} amplified from the PZA31-P_{tet}-M2-GFP plasmid replaced the *kan*^{r} gene in the pEcCas plasmid via λRed recombination method, resulting in the CmPcas plasmid. Primer information is detailed in Table S4.

Strain construction

The *seqA*-, and *hns*-titratable strains were constructed as previously described (Zheng et al., 2016). Briefly, after transforming pSIM5 plasmid into MG1655 cells, the P_{tet}-*tetR*-driven *seqA* or *hns* cassette was inserted at the *attB* site on the genome, and then the native gene was replaced with the *kan*^{r} gene amplified from plkml plasmid.

For the construction of *dnaA*-titratable strain, we first inserted the P_{tet}-*tetR cassette* into the *intS* site via CRISPR/Cas9-λRed genome editing system (Jiang et al., 2015) by targeting 20-nucleotide sequence (tcttcctgcagaccagatcc). Then applying the λRed recombination systems in the CmPcas plasmid, the *bla*:P_{tet}-*dnaA* cassette amplified from the pMD19-RdnaA plasmid via overlap PCR, was inserted between the *yid*A and *yid*X genes, and the negative P_{native}-*dnaA* was replaced with the T_3-Kan-T_1 cassette amplified from the p15A-RdnaA plasmid.

In order to delete the native *lacZ* gene in the genome of the RdnaA1, Rhns1 and MG1655 cells, the homologous recombination fragment amplified from the genome of CL1 strain, was used to knock out the native *lac* operon via CRISPR/Cas9-λRed editing system (Jiang et al., 2015) by targeting 20-nucleotide sequence (cttccggctcgtatgttgtg).

For the construction of DnaA shut-down strain (CRidnaA1), the P_{J23119}-$sgRNA_{dnaA}$:P_{J23100}-*tetR*:P_{tet}-*dUn1Cas12f1* cassette was amplified from the P_CRidnaA1 plasmid and flanked with homologous sequences to the *asn*A and *via*A gene. This cassette was then inserted into the MG1655 genome using

CRISPR/Cas9-λRed editing system, targeting the 19-nucleotide sequence (aagccgcctgctcagacgc). The CPP00458 plasmid, kindly provided by the Xiongfei Fu lab, contains the Un1Cas12f1 variant, which carries mutations D143R, T147R, D326A, and K330R that abolish its DNA-cleaving activity. However, it retains the ability to bind DNA in a sgRNA-guided manner, thereby inhibiting the expression of the target gene.

All primers for the construction of DNA fragments are detailed in Table S4.

Growth conditions

Cells for strain construction were grown in Luria-Bertani (LB) medium with appropriate antibiotics: ampicillin (100 μg·ml^{-1}), kanamycin (50 μg·ml^{-1}), spectinomycin (50 μg·ml^{-1}), chloramphenicol (25 μg·ml^{-1}), based on plasmid presents. For titratable strains, 10 ng·ml^{-1} anhydrotetracycline (aTc) was added during strain construction and seed culture preparation. Seed cultures were initiated by inoculating 3–6 individual colonies from an LB agar plate into 14 ml round-bottom test tubes containing 2 ml of the desired medium for overnight growth.

For physiological phenotypic characterization, all cells were cultivated at 37°C with shaking at 150 rpm in a water bath shaker. The *dnaA*-, *seqA*- and *hns*-titratable cells were characterized under varying aTc concentrations in rich defined medium supplemented with glycerol (M6). *hns*-titratable cells were also characterized in rich defined medium supplemented with glucose (M1). When strains contained reporter plasmid, 25 μg·ml^{-1} chloramphenicol was added. The autoregulated-*dnaA* strain (MGCL1) with a reporter plasmid, was tested in seven different media: M1 (MOPS + EZ + AUCG + Glucose), M2 (MOPS + EZ + Glucose), M3 (MOPS + EZ + AUCG + Gluconate), M6 (MOPS + EZ + AUCG + Glycerol), M12 (MOPS + EZ + Glycerol), M13 (MOPS + CAA + Glycerol), and M18 (MOPS + Glucose). Detailed medium compositions were provided previously (Zheng et al., 2020).

Steady-state growth was established as previously described(Zheng et al., 2020) by culturing cells for ~10 generations in exponential growth phase with ~15-fold dilution at OD_{600} ~0.2, using the same medium supplemented with antibiotic or aTc as required. OD_{600} measurements were taken at consecutive time points using a spectrometer (Genesys 10s, Thermo Fisher Scientific), and the growth rate (or doubling time) λ was calculated by fitting the data to an exponential growth curve. Samples for determination of population-averaged cell mass ($\bar{m}$) and cellular origin number ($\bar{o}$), quantification of mRNA levels, and mRNA fluorescence in situ hybridization (FISH) were collected when OD_{600} reached ~0.2.

Measurements of population-averaged cellular mass ($\bar{m}$), cellular *oriC* number ($\bar{o}$), the initiation to division period (C+D), and initiation mass (m_i)

The population-averaged cell mass ($\bar{m}$), cellular *oriC* number ($\bar{o}$), and initiation mass (m_i) were calculated as described previously(Zheng et al., 2020). Briefly, $\bar{m}$ was determined by dividing the OD_{600} by the cell concentration (OD_{600} ml per 10^9 cells). For cell counting, samples were collected in precooled cell count buffer (0.9% NaCl with 0.12% formaldehyde, filtered with a 0.22 μm filter) and stained with 1 μg·ml^{-1} DAPI in the same buffer. Cell number concentration was measured by counting the DAPI-stained particles using flow cytometry equipped with 405 nm laser (CytoFLEX, Beckman Coulter Life Sciences). The $\bar{o}$ was calculated based on the classical run-out experiments(Zheng et al., 2020). In brief, cell suspensions were treated with 500 μg·ml^{-1} rifampicin and 30 μg·ml^{-1} cephalexin to inhibit new initiation and cell division, respectively, and maintained for 2-3 mass doublings to complete ongoing replication. Cells were fixed with 70% precooled absolute ethanol, and treated with stain buffer (20mM Tris-HCl, pH 8.0, 130 mM NaCl, 10 ng·ml^{-1} DAPI). Using the same flow cytometry, we measured the cellular origin distribution based on DAPI signaling, from which $\bar{o}$ was calculated.

453 C+D was calculated based on the equation: C+D = ln($\bar{o}$)/λ. m_i was calculated based on the equation:
454 $m_i = \frac{\bar{m}}{\bar{o}} \times \frac{1}{ln2}$ (Bremer et al., 1979; Si et al., 2017; Zheng et al., 2016).

455 **Screening of the synthetic promoter library**

456 After transforming the reporter plasmid into *dnaA*-titratable cells, the seed culture was cultivated in
457 M6 medium with 10 ng·ml^{-1} aTc, then diluted 1:180 in fresh medium containing either 0.5 or 50 ng·ml^{-1}
458 aTc and cultivated at 37 °C and 800 r.p.m. in a digital thermo-shaker (AOSHENG) using flat-bottom 96-
459 well plates (Corning). Following approximately 4 hours of pre-cultivation, the cultures were diluted
460 1:180 in fresh medium with the same aTc concentration. The OD_{600} and GFP fluorescence intensity
461 were continuously monitored during cell growth using a Synergy H1 microplate reader (BioTek). The
462 non-fluorescent strain (MG1655) cultured in 180 ul of M6 medium for each experiment was used to
463 subtract the background fluorescence. For OD_{600} between 0.1 and 0.2, the repression fold change
464 was calculated by dividing the mean fluorescence intensity per OD_{600} of the cells grown with 0.5
465 ng·ml^{-1} aTc induction by the corresponding intensity for cells grown with 50 ng·ml^{-1} aTc induction.

466 **Quantitative real-time PCR**

467 Quantitative real-time PCR was performed using a protocol similar to previously described (Zheng et
468 al., 2016). Briefly, RNA was stabilized using Bacteria Protect Reagent (Qiagen) and extracted using
469 RNeasy mini kit (Qiagen). 500 ng RNA was reverse transcribed (TAKARA), and the resulting cDNA
470 samples were diluted 1:25 with PCR-grade water. Quantitative real-time PCR was carried out on a
471 qTower3 (Analytikjena) or CFX Connect system (Bio-Rad), using the following program: 30 s at 95 °C,
472 followed by 40 cycles of denaturation (5 s at 95 °C), annealing, and elongation (30 s at 58 °C). Primer
473 sequences were listed in Table S4. The *rpoA* gene was used as the reference gene.

474 ***lacZ* and *dnaA* mRNA fluorescence in situ hybridization (FISH)**

475 FISH for *lacZ* or *dnaA* mRNA was performed using a method similar to previously described (Skinner
476 et al., 2013). Briefly, antisense DNA oligo probes were designed against *lacZ* or *dnaA*, and synthesized
477 with TAMRA labeling at the 3' end. The sequences of probes targeting *lacZ* or *dnaA* are either as
478 previously described(Skinner et al., 2013) or listed in Table S5. 27 ml steady-state growth culture
479 (OD_{600}~0.2) was fixed by direct adding 3 ml of 37 % (vol/vol) formaldehyde, following by incubation
480 for 30 min at room temperature with gentle mixing using a nutator. The fixed cells were collected by
481 centrifugation at 600 g for 8 minutes, and washed twice with 1 ml RNase-free PBS. The cell pellet was
482 resuspended in 300 µl DEPC water, and 700 µl precooled absolute ethanol was added to permeabilize
483 the cells for 1 hour at room temperature in the nutator. After permeabilization, the cells were divided
484 into two equal parts for characterization of *lacZ* or *dnaA* mRNA as needed. Hybridization was
485 performed as described previously(Skinner et al., 2013), with the stringency of the hybridization and
486 wash solutions adjusted by changing the concentration of formamide, 30 % for *dnaA* probes and 40 %
487 for *lacZ* probes. After hybridization, the cells were washed with the appropriate wash solution and
488 prepared for imaging.

489 **Cell imaging and cell size parameters measurement**

490 For imaging, 3 µl of cell suspension was pipetted onto the center of a 24×60-mm coverslip. A thin
491 1.5 % agarose pad (prepared with 1xPBS) was then placed on top of the cell suspension droplet.
492 Fluorescent and phase images were acquired using an inverted microscope (IX-83, Olympus)
493 equipped with a 100x oil objective (Olympus), an automated xy-stage (ASI, MS2000), and a sCMOS
494 camera (Prime BSI, photometrics). Fluorescence excitation was performed as previously described
495 (Xia et al., 2022). Solid-state lasers (Coherent OBIS: 405–100 LX, 561–100 LS) and Semrock emission
496 bandpass filters (445/40 nm for DAPI and 598/25 nm for RFP) were used for excitation and collecting
497 fluorescent signals.

498 Images were aligned with phase contrast channel by selecting at least six pairs of common control
499 points and applying a geometric transformation using the MATLAB imwarp function. This allowed for
500 adjustment of the cell masks in the RFP or DAPI channel. A customized ImageJ -based image-
501 processing package, MicrobeJ (v5.13I$_1$) plugin for Fiji (Ducret et al., 2016), was used to contour cells
502 and calculate cell size parameters and fluorescence intensity, including the mean cell width, cell
503 length, and cell area from phase-contrast images. The cell volume was calculated using a cylinder-
504 plus-two-hemispheres geometry. The total RFP intensity per cell volume, corrected for background
505 subtraction, was then used to estimate the mRNA concentration of *lacZ* or *danA*.

506 **Characterization of cell cycle-dependent fluctuations in DnaA activity**

507 Data filtering was first performed based on the intensity of the DAPI fluorescence signal. To eliminate
508 non-cell regions resulting from incorrect segmentation of the phase contrast images, only DAPI-
509 positive cells were included in the analysis. To further minimize the potential impact of variability in
510 fixation, permeabilization, and wash efficiencies, which could affect the TAMRA fluorescence signal
511 (representing the mRNA FISH signal), only cells with mean DAPI signals within the 95% confidence
512 intervals were included in the subsequent analysis.
513 The concentration of the *lacZ* mRNA ($[mZ]$) can be expressed as $[mZ] = J/\delta_Z$, where δ_Z is the
514 degradation rate and J is the mRNA synthesis flux. J is in turn given by the promoter on-rate (k),
515 the RNAP concentration ($[RNAP]$), and the concentration of the *lacZ* gene ($[G_Z]$). Assuming that the
516 factors δ_Z, [RNAP], and $[G_Z]$ are the same between the two strains with P_{syn66} and P_{con} driving *lacZ*,
517 then the ratio of the mRNA concentration obtained at each point of the cell cycle gives the ratio of
518 the promoter on-rates, k_{Psyn66} and k_{Pcon}. Since a constitutive promoter is non-responsive to DnaA
519 activity, k_{con} is independent of cell cycle and we can obtain DnaA activity regulated promoter
520 activity as $k_{syn66} = \frac{[mZ](\mathrm{P_{syn66}})}{[mZ](\mathrm{P_{con}})}$, then the DnaA activity is denoted as k_{syn66}^{-1}.
521 The concentration of the *lacZ* mRNA were binned based on cell volume, with a bin size of 0.1 μm^3,
522 was used to determine $[mZ]_{(P\mathrm{syn66})}$ and $[mZ]_{(P\mathrm{con})}$. The relation between $[mZ]_{(P\mathrm{con})}$ and cell volume
523 was smoothed using the MATLAB smooth function, and from this, k_{syn66} was deduced.
524 Based on the DnaA activity oscillations, the cell volume where DnaA activity reaches maximum (V^*)
525 was calculated during a representative birth-to-division cell cycle. The cell volume distribution was
526 used to calculate the number of cells in each volume-doubling range. The range containing the highest
527 cells was considered the representative birth-to-division cell cycle and was shaded in gray (Fig. S2 D).
528 From this, V^* was obtained.

529 **Calculation of cell volume at the time of replication initiation (V_i)**

530 Cell volume at the time of replication initiation (V_i) was calculated based on population-averaged cell
531 volume ($\bar{V}$), and the population-averaged cellular *oriC* number ($\bar{o}$). The equation used for this
532 calculation is as follows:

533 $$V_i = v_i \times N_{oriC}^{ini.} = \frac{\bar{V}}{\bar{o}} \times \frac{1}{ln2} \times 2^{\lfloor log_2^{\bar{o}} \rfloor}$$

534 where v_i is the initiation volume by definition, i.e. cell volume per *oriC* at the time of replication
535 initiation(Bremer et al., 1979; Si et al., 2017; Zheng et al., 2016). $\bar{V}$ was obtained by analyzing the
536 phase contrast images, $\bar{o}$ was obtained by run-out experiments (Zheng et al., 2020). $N_{oriC}^{ini.}$ is the
537 cellular *oriC* number at the time of replication initiation. $\lfloor \log_2 \bar{o} \rfloor$ denotes the floor function of
538 $\log_2 \bar{o}$.

539 **DnaA shut-down experiment**

540 To shut-down DnaA expression, steady-state growth of the CRidnaA1 cells was first established after
541 ~10 generations of exponential growth in M1 medium. At OD$_{600}$ between 0.15 and 0.2, 24 ml of cell

542 culture was transferred to 12 ml of pre-warmed M1 medium containing 150 ng·ml^{-1} aTc to induce
543 dUn1Cas12f1 expression at time 0. Under the guidance of *sgRNA*$_{dnaA}$, the transcription of *dnaA* gene
544 was inhibited. Samples were collected at various time points to determine population-averaged
545 cellular mass ($\bar{m}$), cellular *oriC* number ($\bar{o}$), and to quantify mRNA levels. When the OD_{600} reached
546 around 0.2, the cultures were diluted about 2-fold with pre-warmed M1 medium containing 50
547 ng·ml^{-1} aTc to maintain adequate nutrition. The steady-state growing MG1655 cells in M1 medium
548 were also collected for quantification of wild-type *dnaA* mRNA levels. Three independent
549 experiments were conducted.

550 **H-NS shift-up experiment**

551 The DnaA activity reporter plasmid P_{syn66}-P_{con}-FPs was transformed into the *hns*-titratable strain
552 (Rhns2), and cells were cultivated overnight in M6 medium containing 10 ng·ml^{-1} aTc and 25 μg·ml^{-1}
553 chloramphenicol for seed culture. Seed cultures were washed and grown in the same medium
554 without aTc for ~10 generations of exponential growth. At an OD_{600} of ~0.2, 40 ml of cell culture was
555 transferred to 20 ml of pre-warmed same medium containing 150 ng·ml^{-1} aTc to induce H-NS
556 expression at time 0. Samples were collected at time points -2, 1, 3, 5, 7, 10, 15, 20, 25, and 30 minutes
557 for the determination of population-averaged cellular mass ($\bar{m}$), cellular *oriC* number ($\bar{o}$), and
558 quantification of mRNA levels. Steady-state growing MG1655 in M6 medium were also collected for
559 *hns* mRNA quantification. Three independent experiments were conducted.

560 **Electrophoretic mobility shift assay (EMSA)**

561 The genes encoding *dnaA* and *hns* from the MG1655 genome were individually amplified and cloned
562 into the expression vector pET-28a using primers listed in Table S4. *E. coli* BL21 (DE3) carrying pET-
563 28a-DnaA or pET-28a-H-NS was used for overproduction of His_6-DnaA or His_6-H-NS. For each protein
564 purification, a 1 L culture was induced by the addition of 1 mM IPTG at OD_{600} = 0.4. After 1.5 hours of
565 incubation, cells were harvested by centrifugation (5,000 rpm for 20 min at 4 °C). The pellet was
566 resuspended in 50 ml of buffer A (50 mM Tris-HCl, pH 7.0, 500 mM NaCl, 0.5 mM PMSF, 5 % glycerol).
567 Cell resuspension was lysed on ice for 30 minutes (3 seconds on, 7 seconds off) using a sonicator at
568 4 °C, and cell debris was removed by centrifugation (14,000 rpm for 60 min at 4 °C). Subsequently,
569 the protein was purified from the soluble supernatant by Ni^{2+}-affinity chromatography (HisTrap™ HP
570 Columns; GE Healthcares) with a ÄKTA Pure Protein Purification System. Proteins were collected using
571 gradient elution with buffer B [20 mM Tris-HCl, pH 7.5, 500 mM NaCl, 400 mM imidazole, 5 % glycerol].
572 Eluted proteins were further purified and concentrated by ultrafiltration using Amicon Ultra 10K (for
573 H-NS) and 30K (for DnaA) filters (Millipore). Finally, after overnight dialysis (0.025 μm Membrane
574 Filter; MF-Millipore) at 4 °C, the protein was stored in buffer C [45 mM Hepes-KOH, pH 7.6, 600 mM
575 potassium glutamate, 1 mM DTT, 10 mM magnesium acetate, 0.5 mM EDTA, 20 % glycerol].
576 Judgement by SDS/PAGE with Coomassie Brilliant blue staining, the purity of each protein was >90 %.
577 For the experiments where H-NS acts on the *datA* bound by DnaA, the purified DnaA, *datA* and ATP
578 were first incubated in buffer D (20 mM Tris-HCl, pH 7.5, 150 mM potassium glutamate, 10 mM
579 magnesium acetate, 8 mM DTT) at 20 °C for 10 min. Then the H-NS was added to buffer D (15 μl)
580 which contained DnaA-*datA* complexes and incubated for additional 10 min at 20 °C. The final
581 complexes were separated by electrophoresis in 2 % (wt/vol) agarose gel at 80 V for 70 min in Tris-
582 Borate buffer, followed by staining with SYBR Safe (Invitrogen).

583 **Titration model**

584 In the titration model, we posit that the cell mass grows exponentially according to the differential
585 equation $\frac{dV}{dt} = \lambda V$, where V represents the volume of the cell and $\lambda = 1.54\ h^{-1}$(corresponding to

doubling time of 27 min) is the growth rate. Concurrently, the number of total DnaA protein (A) increases at a rate proportional to the cell's mass, described by $\frac{dA}{dt} = \alpha_A V$, with $\alpha_A = 300\ h^{-1}\mu m^{-3}$ denoting the synthesis rate per unit volume. The chromosome's structure is abstracted as a vector representing the copy numbers of uniformly distributed sites along its length, and the number of DnaA-boxes (A_b) is quantified by summing the boxes number at their respective locations. In this model, 300 DnaA-boxes are evenly distributed on the chromosome while an additional 100 DnaA-boxes are located near the *oriC*. This arrangement approximates a head-weighted distribution of DnaA-boxes and helps prevent over-initiation(Hansen et al., 1991). Binding of DnaA proteins to these DnaA-boxes allows us to calculate the concentration of free DnaA as $[A_f] = (A - A_b)/V$, under condition of $(A - A_b) \geq 0$. DNA replication commences once the concentration of free DnaA exceeds a critical threshold $[A_f^c] = 10\ \mu m^{-3}$: $[A_f] > [A_f^c]$. 10 min sequestration time was set after replication initiation to mimic the sequestration time(Campbell & Kleckner, 1990).
To explore the dynamics of the *oriC* number following the cessation of *dnaA* expression, we can set the synthesis rate to be zero $\alpha_A = 0$. To simulate the dependence of initiation mass on *dnaA* expression, α_A varies from 60 $h^{-1}\mu m^{-3}$ to 3840 $h^{-1}\mu m^{-3}$.

Extrusion model

The extrusion model was formulated following the titration model, with an additional extruder introduced as a protein with synthesis rate $\alpha_H = 180\ h^{-1}\mu m^{-3}$ and dynamics $dH/dt = \alpha_H V$. The additional extruder competes the DnaA-boxes with DnaA proteins, with higher affinity to DnaA-boxes. So that it can displace DnaA from the DnaA-boxes, leading to a revised calculation for free DnaA concentration as $[A_f] = (A - (A_b - H))/V$, under condition of $(A_b - H) \geq 0$ and $(A - (A_b - H)) \geq 0$. To get stochastic modelling for adder phenomenon, we introduced white noises on cell mass growth rate and the DnaA synthesis rate at each replication cycle: $\lambda = \lambda_0 + \eta\lambda_0$, $\alpha_A = \alpha_0 + \eta\alpha_0$ where $\lambda_0 = 0.66\ h^{-1}, \alpha_0 = 300\ h^{-1}\mu m^{-3}$ and $\eta = 0.1$ representing white noise. This extrusion model exhibits consistent performance under various parameter ranges.

DnaA-ATP/DnaA-ADP switch model

The switch model was simulated following the idea of LDDR model proposed by Berger *et al.* (Berger & Wolde, 2022). The formulations of the DnaA-ATP fraction dynamics is:

$$\frac{df}{dt} = \left(\frac{\alpha_l}{[D]_T}V + \frac{\alpha_{d1}}{[D]_T}N_{d1} + \frac{\alpha_{d1}}{[D]_T}N_{d2}\right)\frac{1-f}{\frac{K_D}{[D]_T} + 1 - f} - \left(\frac{\beta_{datA}}{[D]_T} + \frac{\beta_{rida}}{[D]_T}\right)N_o\frac{f}{\frac{K_D}{[D]_T} + f} + \frac{\alpha_A}{[D]_T}\lambda(1-f)$$

In this equation $[D]_T = 400\mu m^{-3}$ is the concentration of total DnaA proteins in a cell $\alpha_l = 750h^{-1}$ is the activation rate of DnaA-ATP by lipid; $\alpha_{d1} = 100\ h^{-1}$, $\alpha_{d2} = 643\ h^{-1}$ are the activation rate of DnaA-ATP by the DARS1 and DARS2 sites; $\beta_{datA} = 600\ h^{-1}, \beta_{rida} = 500\ h^{-1}$ are the deactivation rate of DnaA-ATP by *datA* and RIDA; $K_D = 50\mu m^{-3}$ the dissociation constant of DnaA activation and deactivation; N_{d1}, N_{d2}, N_o are copy number of DARS1, DARS2 and *oriC* sites extracted dynamically from the DNA copy number vector; $\alpha_A = 300\ h^{-1}\mu m^{-3}$ is the DnaA expression level. The DNA replication initiation was determined when f reaches a threshold $f_C = 0.75$ (Berger & Wolde, 2022). To simulate the *dnaA* shut-down, we simply deleted the term of *dnaA* synthesis ($\lambda(1-f)$).

Titration-switch model and titration-switch-extrusion model

In the integrated model combining titration and switch mechanisms, replication initiation is triggered when the concentration of free DnaA-ATP $[A_{ATP}^f]$ exceeds a threshold $[A_{ATP}^{fc}]$. The concentration of

free DnaA-ATP is titrated by the DnaA-boxes on the chromosome as in the titration model, with $[A_{ATP}^{f}] = (A_{ATP} - A_b)/V$, under condition of $(A_{ATP} - A_b) \geq 0$. The parameters related to the titration dynamics remain consistent with those described in earlier sections of titration model.

The dynamics of total DnaA-ATP (A_{ATP}) is governed by both expression and conversion processes as described in Berger *et al*. (Berger & Wolde, 2022). According to this framework, the lipid and DARS systems facilitate the conversion of DnaA-ADP to DnaA-ATP at constant rates, while the *datA* site and RIDA systems also play a role in converting DnaA-ATP to DnaA-ADP, again at fixed rates. Additionally, the synthesis of new DnaA proteins provides another source of DnaA-ATP.

To be specific, DNA replication initiates was set when the concentration of free DnaA-ATP, $[A_f^{ATP}] = (A^{ATP} - A_b)/V$ exceeds a threshold $[A_f^c]$. The dynamics of total DnaA number in a cell A followed $\frac{dA}{dt} = \frac{\phi_{P0}\lambda V}{1+\left([A_f^{ATP}]/K_D^P\right)^n}$, and the dynamics of total DnaA-ATP number A^{ATP} followed:

$$\frac{dA^{ATP}}{dt} = (\alpha_l V + \alpha_{d1}N_{d1} + \alpha_{d2}N_{d2})\frac{[A^{ADP}]}{K_D + [A^{ADP}]} - (\beta_{datA} + \beta_{rida})N_o\frac{[A_f^{ATP}]}{K_D + [A_f^{ATP}]} + \frac{\phi_{P0}\lambda V}{1 + \left([A_f^{ATP}]/K_D^P\right)^n}$$

where the three terms on the right represent activation and deactivation of DnaA-ATP and new synthesis of DnaA-ATP. In these equations $[A^{ADP}] = \frac{(A - A^{ATP})}{V}$ is the concentration of DnaA-ADP; $[D_T] = 400\ \mu m^{-3}$ is the total DnaA concentration; $K_D^P = 400\ \mu m^{-3}$ is the dissociation constant of DnaA promoter; ϕ_{p0} is the DnaA protein ratio relative to all proteins, which is proportional to α_A and ranges from 0.002% to 0.1%; $n = 5$ is the cooperativity of *dnaA* expression; The same activation/deactivation rates and dissociation constants of DnaA ($\alpha_l, \alpha_{d1}, \alpha_{d2}, \beta_{datA}, \beta_{rida}, K_D$) are used as in the switch model; N_{d1}, N_{d2}, N_o are copy number of DARS1, DARS2 and *oriC* sites extracted dynamically from the DNA copy number vector. To get a good fit of the initiation mass-*dnaA* expression relation, high threshold of free DnaA-ATP concentration was applied, $[A_{ATP}^{fc}] = 200\ \mu m^{-3}$.

To simulate the titration-switch-extrusion model, we incorporated the extruder as described in the extrusion model, where its amount was given by $H = \alpha_H V$. The concentration of free DnaA-ATP was then calculated as $[A_{ATP}^{f}] = (A_{ATP} - (A_b - H))/V$, under condition of $(A_b - H) \geq 0$ and $(A_{ATP} - (A_b - H)) \geq 0$. To explore the best fit of continuous DNA replication rounds following *dnaA* shut-down, $\alpha_H = 550\ h^{-1}\mu m^{-3}$ is used.

All parameters are summarized in Tables S6.

Data availability

All data supporting the findings of this work are available from the corresponding author upon request. Source data are provided with this paper.

Code availability

Simulation data can be generated using the custom-made code and the parameter sets provided. The code is publicly available at https://github.com/BaiYangBqdq/dynamics_of_biomass_DNA_coordination.

Acknowledgements

We thank numerous colleagues for discussions. We sincerely thank Dr. Aiguo Xia for his help with microscopy, and Dr. Sheng Yang for providing valuable suggestions on CRISPR-Cas9 system. Special

666 thanks to Drs. Pan Chu and Yeqing Zong for kindly gifting us the CPP00458 and pPT plasmids. This
667 research was financially supported by the National Natural Science Foundation of China (32025022,
668 32230062), Strategic Priority Research Program of the Chinese Academy of Sciences (XDB0480000),
669 Joint NSFC-ISF Research Grant (32061143021) to C.L., US-Israel Binational Science Foundation
670 (2017004) and Israel Science Foundation-NSCF joint research program (3320/20) to A.Z. National
671 Natural Science Foundation of China (32170042), National Key R&D Program of China
672 (2024YFA0916403), Youth Innovation Promotion Association CAS (number 2022369) to H.Z., National
673 Key R&D Program of China (2021YFA0910703) to Y.B.; National Centre for Engineering Biology (NRF-
674 MSG-2023-0003) and National University of Singapore (NUHSRO/2024/064/NUSMed/05/ SynCTI2.0)
675 to M.W.C.

676 Author contributions

677 C.L. conceived the study and supervised all research. D.L. and T.W. designed the synthetic promoter
678 library, validated reporters, and performed mRNA FISH experiments with assistance from H.Z. D.L.,
679 H.Z., and H.C. characterized H-NS phenotypes and conducted shift experiments. D.L. and X.H.
680 executed DnaA shutdown experiments. C.L. and T.H. developed the extrusion model concept; Y.B.,
681 H.Z., and Z.Z. implemented mathematical modeling and simulations. A.Z. and M.W.C. contributed to
682 data interpretation and manuscript refinement. All authors analyzed data, reviewed drafts, and
683 approved the final manuscript. D.L., Y.B. and C.L. led manuscript writing.

684 Competing interests

685 The authors declare no competing interests.

References

Balakrishnan, R., Mori, M., Segota, I., Zhang, Z., Aebersold, R., Ludwig, C., Hwa, T. 2022. Principles of gene regulation quantitatively connect DNA to RNA and proteins in bacteria. *Science*, **378**(6624), eabk2066. http://doi.org/10.1126/science.abk2066

Berger, M., Wolde, P.R.t. 2022. Robust replication initiation from coupled homeostatic mechanisms. *Nat. Commun.*, **13**(1), 6556. http://doi.org/10.1038/s41467-022-33886-6

Bintu, L., Buchler, N.E., Garcia, H.G., Gerland, U., Hwa, T., Kondev, J., Kuhlman, T., Phillips, R. 2005a. Transcriptional regulation by the numbers: applications. *Curr. Opin. Genet. Dev.*, **15**(2), 125-35. http://doi.org/10.1016/j.gde.2005.02.006

Bintu, L., Buchler, N.E., Garcia, H.G., Gerland, U., Hwa, T., Kondev, J., Phillips, R. 2005b. Transcriptional regulation by the numbers: models. *Curr. Opin. Genet. Dev.*, **15**(2), 116-24. http://doi.org/10.1016/j.gde.2005.02.007

Boye, E., Stokke, T., Kleckner, N., Skarstad, K. 1996. Coordinating DNA replication initiation with cell growth: Differential roles for DnaA and SeqA proteins. *Proc. Natl. Acad. Sci. U. S. A.*, **93**(22), 12206-12211. http://doi.org/10.1073/pnas.93.22.12206

Braun, R.E., O'Day, K., Wright, A. 1985. Autoregulation of the DNA replication gene *dnaA* in *E. coli* K-12. *Cell*, **40**(1), 159-169. http://doi.org/https://doi.org/10.1016/0092-8674(85)90319-8

Bremer, H., Churchward, G., Young, R. 1979. Relation between growth and replication in bacteria. *J. Theor. Biol.*, **81**(3), 533-45. http://doi.org/10.1016/0022-5193(79)90051-1

Campbell, J.L., Kleckner, N. 1990. *E. coli oriC* and the *dnaA* gene promoter are sequestered from dam methyltransferase following the passage of the chromosomal replication fork. *Cell*, **62**(5), 967-79. http://doi.org/10.1016/0092-8674(90)90271-f

Christensen, B.B., Atlung, T., Hansen, F.G. 1999. DnaA boxes are important elements in setting the initiation mass of *Escherichia coli*. *J. Bacteriol.*, **181**(9), 2683-2688. http://doi.org/10.1128/jb.181.9.2683-2688.1999

Dame, R.T., Wyman, C., Goosen, N. 2000. H-NS mediated compaction of DNA visualised by atomic force microscopy. *Nucleic Acids Res.*, **28**(18), 3504-10. http://doi.org/10.1093/nar/28.18.3504

Dillon, S.C., Dorman, C.J. 2010. Bacterial nucleoid-associated proteins, nucleoid structure and gene expression. *Nat. Rev. Microbiol.*, **8**(3), 185-195. http://doi.org/10.1038/nrmicro2261

Donachie, W.D., Blakely, G.W. 2003. Coupling the initiation of chromosome replication to cell size in *Escherichia coli*. *Curr. Opin. Microbiol.*, **6**(2), 146-150. http://doi.org/10.1016/s1369-5274(03)00026-2

Dong, M.J., Luo, H., Gao, F. 2023. DoriC 12.0: an updated database of replication origins in both complete and draft prokaryotic genomes. *Nucleic Acids Res.*, **51**(D1), D117-d120. http://doi.org/10.1093/nar/gkac964

Dorman, C.J. 2004. H-NS: a universal regulator for a dynamic genome. *Nat. Rev. Microbiol.*, **2**(5), 391-400. http://doi.org/10.1038/nrmicro883

Ducret, A., Quardokus, E.M., Brun, Y.V. 2016. MicrobeJ, a tool for high throughput bacterial cell detection and quantitative analysis. *Nat. Microbiol.*, **1**(7), 16077. http://doi.org/10.1038/nmicrobiol.2016.77

Fragkos, M., Ganier, O., Coulombe, P., Méchali, M. 2015. DNA replication origin activation in space and time. *Nat. Rev. Mol. Cell Biol.*, **16**(6), 360-74. http://doi.org/10.1038/nrm4002

Fu, H., Xiao, F., Jun, S. 2023. Bacterial replication initiation as precision control by protein counting. *PRX Life*, **1**(1). http://doi.org/10.1103/prxlife.1.013011

730 Grimwade, J.E., Leonard, A.C. 2021. Blocking, bending, and binding: regulation of initiation of
731 chromosome replication during the *Escherichia coli* cell cycle by transcriptional modulators that
732 interact with origin DNA. *Front. Microbiol.*, **12**. http://doi.org/10.3389/fmicb.2021.732270
733 Hansen, F.G., Atlung, T. 2018. The DnaA tale. *Front. Microbiol.*, **9**.
734 http://doi.org/10.3389/fmicb.2018.00319
735 Hansen, F.G., Christensen, B.B., Atlung, T. 1991. The initiator titration model: computer simulation of
736 chromosome and minichromosome control. *Res. Microbiol.*, **142**(2), 161-167.
737 http://doi.org/https://doi.org/10.1016/0923-2508(91)90025-6
738 Hommais, F., Krin, E., Laurent-Winter, C., Soutourina, O., Malpertuy, A., Le Caer, J.P., Danchin, A.,
739 Bertin, P. 2001. Large-scale monitoring of pleiotropic regulation of gene expression by the
740 prokaryotic nucleoid-associated protein, H-NS. *Mol. Microbiol.*, **40**(1), 20-36.
741 http://doi.org/10.1046/j.1365-2958.2001.02358.x
742 Iuliani, I., Mbemba, G., Lagomarsino, M.C., Sclavi, B. 2024. Direct single-cell observation of a key
743 *Escherichia coli* cell-cycle oscillator. *Sci. Adv.*, **10**(29), eado5398.
744 http://doi.org/10.1126/sciadv.ado5398
745 Jiang, Y., Chen, B., Duan, C., Sun, B., Yang, J., Yang, S. 2015. Multigene editing in the *Escherichia coli*
746 genome via the CRISPR-Cas9 system. *Appl. Environ. Microbiol.*, **81**(7), 2506-2514.
747 http://doi.org/10.1128/aem.04023-14
748 Kaguni, J.M. 2011. Replication initiation at the *Escherichia coli* chromosomal origin. *Curr. Opin. Chem.*
749 *Biol.*, **15**(5), 606-13. http://doi.org/10.1016/j.cbpa.2011.07.016
750 Katayama, T., Kasho, K., Kawakami, H. 2017. The DnaA cycle in *Escherichia coli*: activation, function
751 and inactivation of the initiator protein. *Front. Microbiol.*, **8**.
752 http://doi.org/10.3389/fmicb.2017.02496
753 Khodursky, A., Guzmán, E.C., Hanawalt, P.C. 2015. Thymineless death lives on: new insights into a
754 classic phenomenon. *Annu. Rev. Microbiol.*, **69**, 247-263. http://doi.org/10.1146/annurev-micro-
755 092412-155749
756 Knöppel, A., Broström, O., Gras, K., Elf, J., Fange, D. 2023. Regulatory elements coordinating initiation
757 of chromosome replication to the *Escherichia coli* cell cycle. *Proc. Natl. Acad. Sci. U. S. A.*, **120**(22),
758 e2213795120. http://doi.org/10.1073/pnas.2213795120
759 Løbner-Olesen, A., Skarstad, K., Hansen, F.G., von Meyenburg, K., Boye, E. 1989. The DnaA protein
760 determines the initiation mass of *Escherichia coli* K-12. *Cell*, **57**(5), 881-9.
761 http://doi.org/10.1016/0092-8674(89)90802-7
762 Lu, M., Campbell, J.L., Boye, E., Kleckner, N. 1994. SeqA: a negative modulator of replication initiation
763 in *E. coli*. *Cell*, **77**(3), 413-26. http://doi.org/10.1016/0092-8674(94)90156-2
764 Lutz, R., Bujard, H. 1997. Independent and tight regulation of transcriptional units in *Escherichia coli*
765 via the LacR/O, the TetR/O and AraC/I1-I2 regulatory elements. *Nucleic Acids Res.*, **25**(6), 1203-10.
766 http://doi.org/10.1093/nar/25.6.1203
767 Mäkelä, J., Papagiannakis, A., Lin, W.H., Lanz, M.C., Glenn, S., Swaffer, M., Marinov, G.K., Skotheim,
768 J.M., Jacobs-Wagner, C. 2024. Genome concentration limits cell growth and modulates proteome
769 composition in *Escherichia coli*. *Elife*, **13**. http://doi.org/10.7554/eLife.97465
770 Ohbayashi, R., Hirooka, S., Onuma, R., Kanesaki, Y., Hirose, Y., Kobayashi, Y., Fujiwara, T., Furusawa, C.,
771 Miyagishima, S.-y. 2020. Evolutionary changes in DnaA-dependent chromosomal replication in
772 cyanobacteria. *Front. Microbiol.*, **11**. http://doi.org/10.3389/fmicb.2020.00786
773 Ozaki, S., Katayama, T. 2012. Highly organized DnaA-*oriC* complexes recruit the single-stranded DNA

774 for replication initiation. *Nucleic Acids Res.*, **40**(4), 1648-65. http://doi.org/10.1093/nar/gkr832
775 Pountain, A.W., Jiang, P., Yao, T., Homaee, E., Guan, Y., McDonald, K.J.C., Podkowik, M., Shopsin, B.,
776 Torres, V.J., Golding, I., Yanai, I. 2024. Transcription–replication interactions reveal bacterial
777 genome regulation. *Nature*, **626**(7999), 661-669. http://doi.org/10.1038/s41586-023-06974-w
778 Saggioro, C., Olliver, A., Sclavi, B. 2013. Temperature-dependence of the DnaA-DNA interaction and
779 its effect on the autoregulation of *dnaA* expression. *Biochem. J.*, **449**, 333-341.
780 http://doi.org/10.1042/bj20120876
781 Sekimizu, K., Bramhill, D., Kornberg, A. 1987. ATP activates DnaA protein in initiating replication of
782 plasmids bearing the origin of the *E. coli* chromosome. *Cell*, **50**(2), 259-265.
783 http://doi.org/https://doi.org/10.1016/0092-8674(87)90221-2
784 Si, F., Le Treut, G., Sauls, J.T., Vadia, S., Levin, P.A., Jun, S. 2019. Mechanistic origin of cell-size control
785 and homeostasis in bacteria. *Curr. Biol.*, **29**(11), 1760-1770.e7.
786 http://doi.org/10.1016/j.cub.2019.04.062
787 Si, F., Li, D., Cox, S.E., Sauls, J.T., Azizi, O., Sou, C., Schwartz, A.B., Erickstad, M.J., Jun, Y., Li, X., Jun, S.
788 2017. Invariance of initiation mass and predictability of cell size in *Escherichia coli*. *Curr. Biol.*, **27**(9),
789 1278-1287. http://doi.org/10.1016/j.cub.2017.03.022
790 Skinner, S.O., Sepulveda, L.A., Xu, H., Golding, I. 2013. Measuring mRNA copy number in individual
791 *Escherichia coli* cells using single-molecule fluorescent *in situ* hybridization. *Nat. Protoc.*, **8**(6),
792 1100-1113. http://doi.org/10.1038/nprot.2013.066
793 Speck, C., Weigel, C., Messer, W. 1999. ATP- and ADP-DnaA protein, a molecular switch in gene
794 regulation. *EMBO J.*, **18**(21), 6169-6176. http://doi.org/10.1093/emboj/18.21.6169
795 Witz, G., van Nimwegen, E., Julou, T. 2019. Initiation of chromosome replication controls both division
796 and replication cycles in *E. coli* through a double-adder mechanism. *Elife*, **8**.
797 http://doi.org/10.7554/eLife.48063
798 Xia, A., Zhang, R., Huang, Y., Ni, L., Pu, L., Li, Y., Yang, S., Jin, F. 2022. An adaptive tracking illumination
799 system for optogenetic control of single bacterial cells. *Appl. Microbiol. Biotechnol.*, **106**(19-20),
800 6775-6784. http://doi.org/10.1007/s00253-022-12177-6
801 Xie, S., Swaffer, M., Skotheim, J.M. 2022. Eukaryotic cell size control and its relation to biosynthesis
802 and senescence. *Annu. Rev. Cell Dev. Biol.*, **38**, 291-319. http://doi.org/10.1146/annurev-cellbio-
803 120219-040142
804 Zaritsky, A., Pritchard, R.H. 1971. Replication time of the chromosome in thymineless mutants of
805 *Escherichia coli*. *J. Mol. Biol.*, **60**(1), 65-74. http://doi.org/10.1016/0022-2836(71)90447-5
806 Zheng, H., Bai, Y., Jiang, M., Tokuyasu, T.A., Huang, X., Zhong, F., Wu, Y., Fu, X., Kleckner, N., Hwa, T.,
807 Liu, C. 2020. General quantitative relations linking cell growth and the cell cycle in *Escherichia coli*.
808 *Nat. Microbiol.*, **5**(8), 995-1001. http://doi.org/10.1038/s41564-020-0717-x
809 Zheng, H., Ho, P.-Y., Jiang, M., Tang, B., Liu, W., Li, D., Yu, X., Kleckner, N.E., Amir, A., Liu, C. 2016.
810 Interrogating the *Escherichia coli* cell cycle by cell dimension perturbations. *Proc. Natl. Acad. Sci. U.*
811 *S. A.*, **113**(52), 15000-15005. http://doi.org/10.1073/pnas.1617932114
812 Zimmerman, S.B. 2006. Cooperative transitions of isolated *Escherichia coli* nucleoids: implications for
813 the nucleoid as a cellular phase. *J. Struct. Biol.*, **153**(2), 160-75.
814 http://doi.org/10.1016/j.jsb.2005.10.011
815 Zong, Y., Zhang, H.M., Lyu, C., Ji, X., Hou, J., Guo, X., Ouyang, Q., Lou, C. 2017. Insulated transcriptional
816 elements enable precise design of genetic circuits. *Nat. Commun.*, **8**(1), 52.
817 http://doi.org/10.1038/s41467-017-00063-z

818 Supplementary information:

819

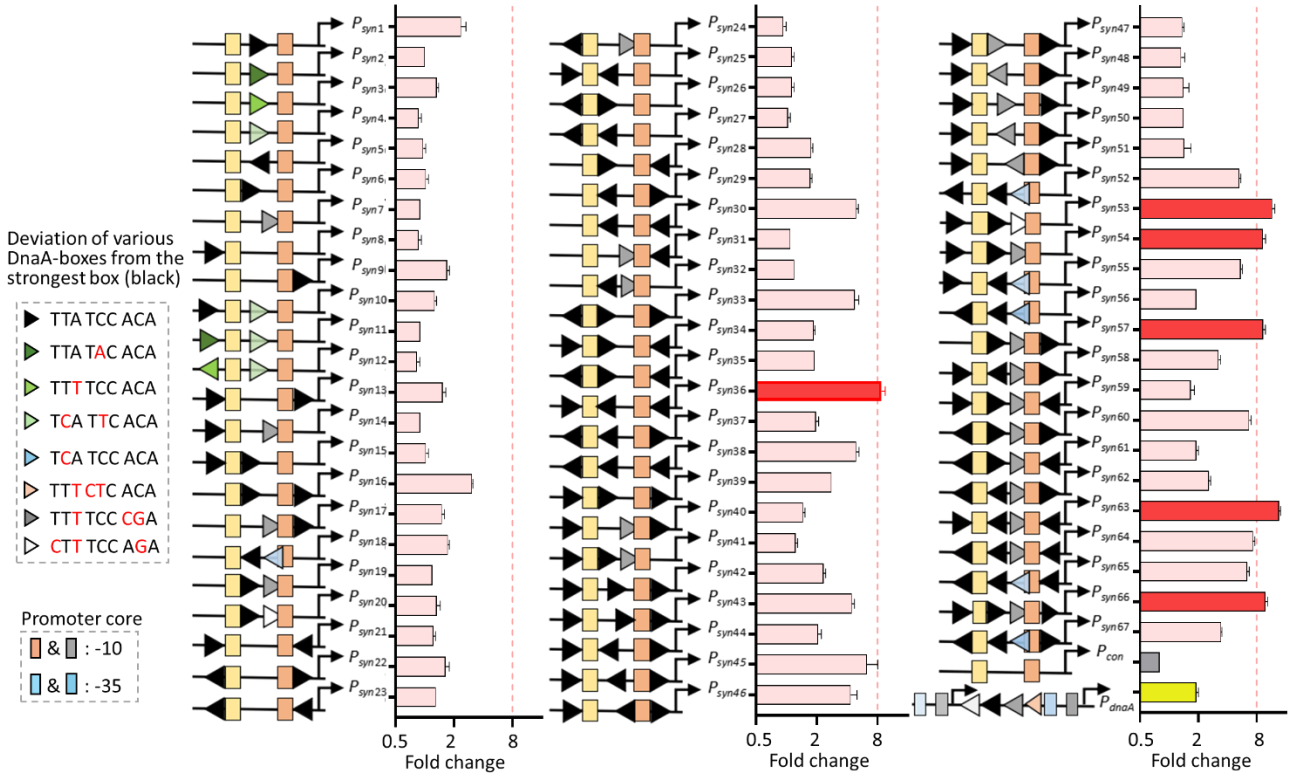

820

821 **Figure S1. Screening a library of synthetic promoters reveals potential candidates to report DnaA**
822 **activity**. For each synthetic promoter, various combinations of DnaA-boxes were inserted near the
823 promoter core, and their repression fold in response to elevated DnaA expression was measured in
824 *dnaA*-titratable cells grown in 0.5 ng·ml^{-1} aTc compared to cells grown in 50 ng·ml^{-1} aTc, using a
825 microplate reader. Error bars represent the standard deviation (SD) of three replicates.

826

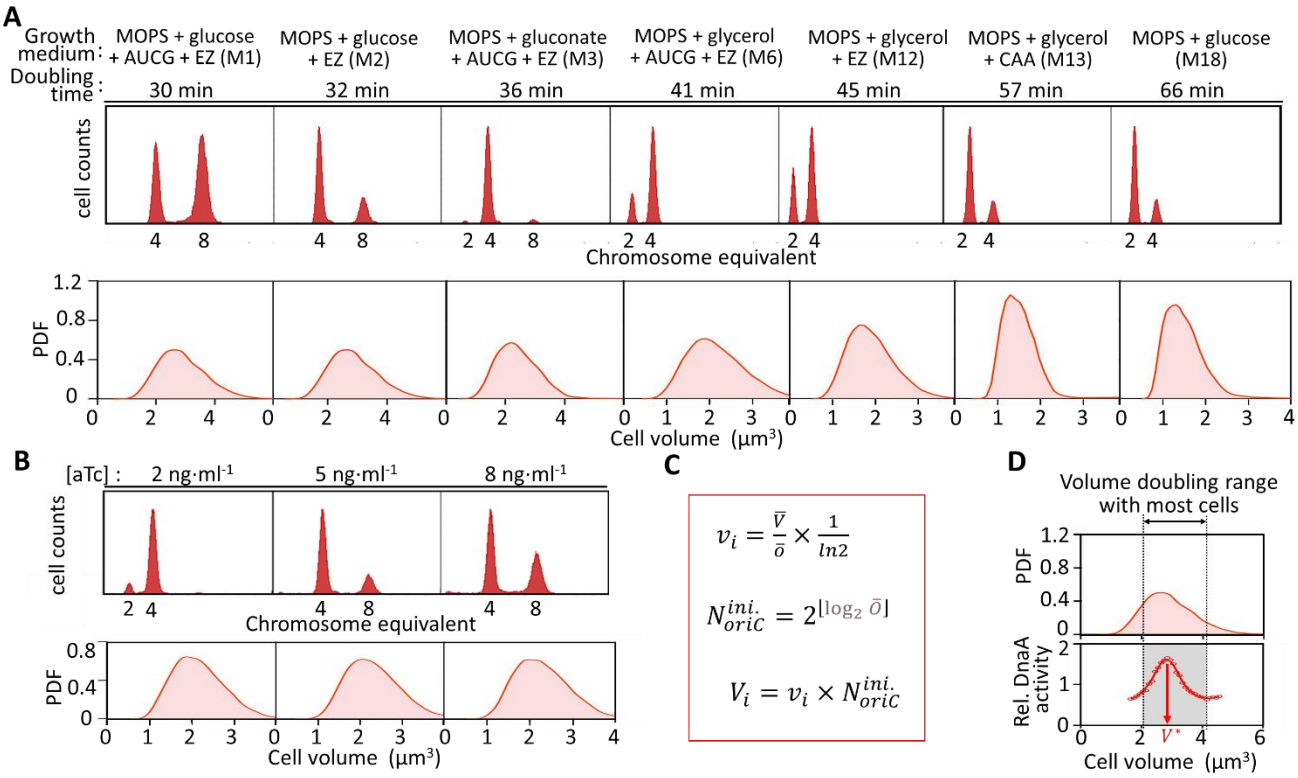

Figure S2. Determination of cell volume at replication initiation and representative birth-to-division cell cycle. (A-B) Distribution of cellular *oriC* content (up) and cell volume (low) for cells shown in Fig.4C cultivated in various growth media with noted doubling time (**A**), and for cells shown in Fig. 4F grown in M6 medium with noted aTc concentrations (**B**). Cellular *ori*C was determined using run-out experiments followed by flow cytometry, and cell volume was obtained from phase-contrast images from mRNA FISH experiments. **(C)** Calculation of the cell volume at replication initiation. Based on panels **A** and **B**, the population-averaged cellular *oriC* content ($\bar{o}$) and cell volume ($\bar{V}$) were determined, then the initiation volume can be deduced accordingly. Additionally, the *oriC* number at the initiation time ($N_{oriC}^{ini.}$) was calculated based on $\bar{o}$. Cell volume at the replication initiation was derived by definition. **(D)** Illustration of the determination of the representative birth-to-division cell cycle for DnaA activity oscillations. The cell volume distribution is analyzed to calculate the number of cells within each volume-doubling range. The range with the most cell counts is defined as the representative birth-to-division cycle, which is shaded in gray.

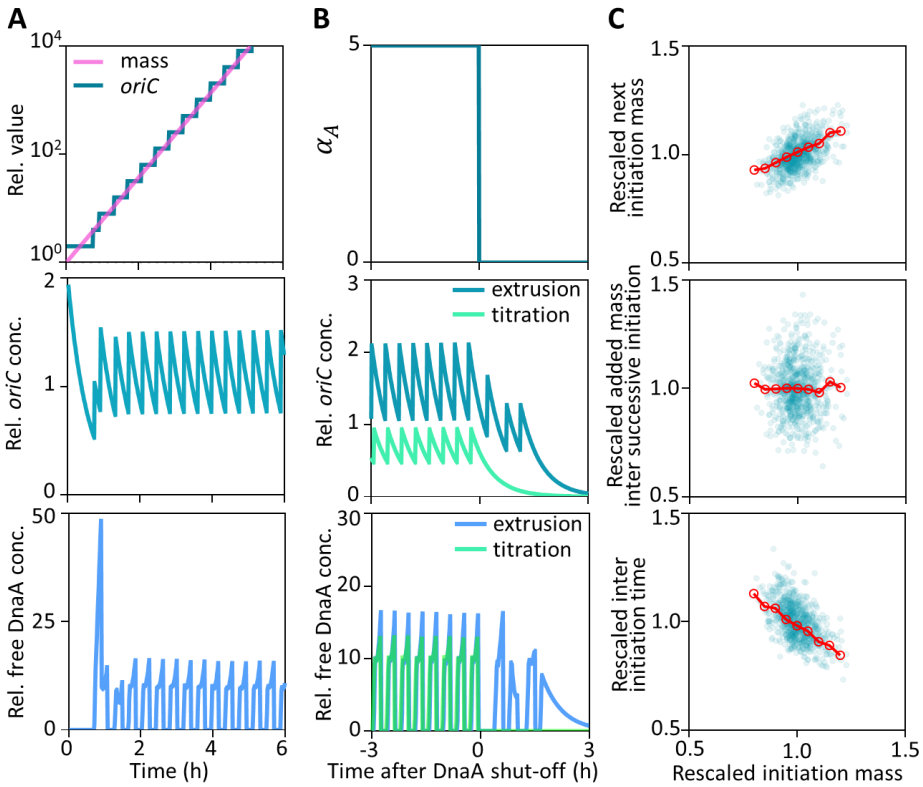

Figure S3. Predictions of the extrusion model. (A) Dynamics of relative total cell mass and *oriC* number (upper panel), *oriC* concentration (middle panel), and free DnaA concentration (lower panel), predicted by a deterministic version of the extrusion model, without considering cell division. **(B)** Simulations of DnaA shut-down. DnaA shut-down was simulated by changing the *dnaA* expression level α_A to 0 (upper panel). During DnaA shut down, dynamics of relative *oriC* concentration (middle panel) and free DnaA concentration (lower panel) predicted by the titration model and extrusion model were plotted and compared. **(C)** Initiation adder phenomenon predicted by the extrusion model. A stochastic version of the extrusion model was simulated. The next initiation mass (upper panel), added mass between successive initiations (middle panel), and added time between successive initiations (lower panel) were plotted against the initiation mass in previous initiation, both normalized to their averages (blue dots, n=820). Mean values were calculated in bins of 0.05 relative initiation mass (red dotted line)

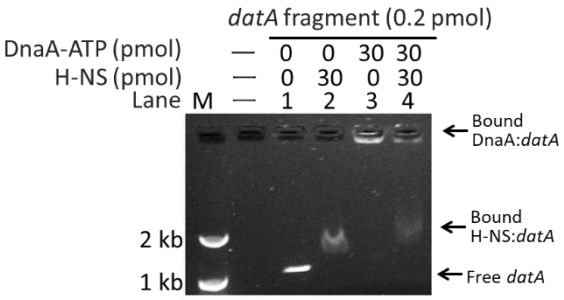

855

856 **Figure S4. H-NS promotes the release of DnaA from the *datA* sequence.** Competitive binding
857 between H-NS and DnaA to *datA* fragments. H-NS and DnaA formed distinct complexes with *datA*,
858 resulting in H-NS:*datA* (lane 2) and DnaA:*datA* (lane 3) complexes. Addition of H-NS to pre-incubated
859 DnaA:*datA* complex resulted in coexistence of both DnaA:*datA* and H-NS:*datA* complexes (lane 4).

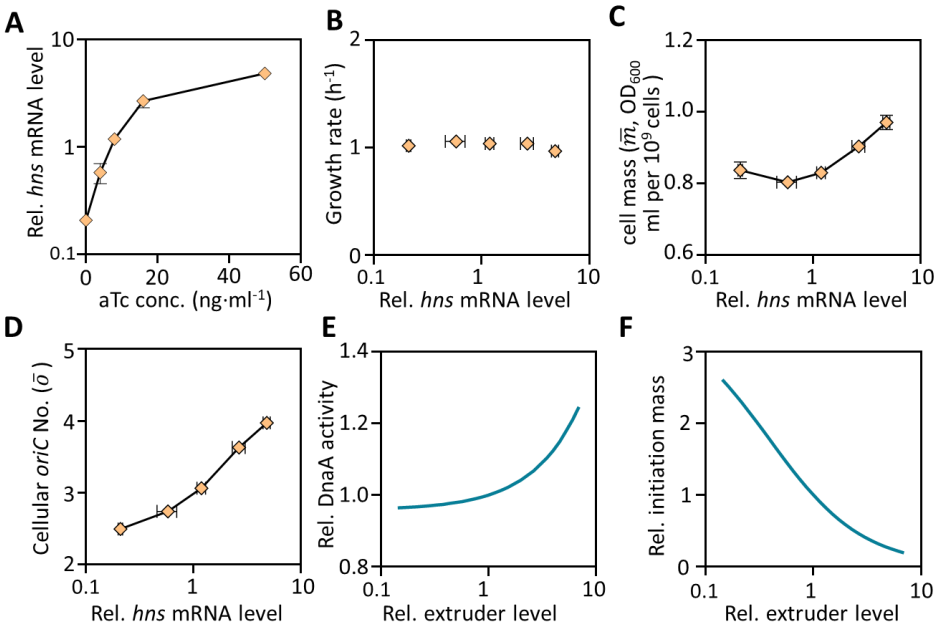

Figure S5. Basic phenotypic characterization of *hns*-titratable cells harboring a DnaA activity reporting plasmid. **(A)** Relative *hns* mRNA levels were measured in steady-state growing cells in rich defined medium supplemented with glycerol at various aTc concentration. Growth rate(**B**), population-averaged cellular mass $\bar{m}$ (**C**), and cellular *oriC* number $\bar{o}$ (**D**) were characterized as a function of *hns* mRNA levels for these steady-state cultures. Relative DnaA activity (represented by free DnaA concentration) (**E**) and initiation mass (**F**) as a function of varying extruder concentration as predicted by the extrusion model.

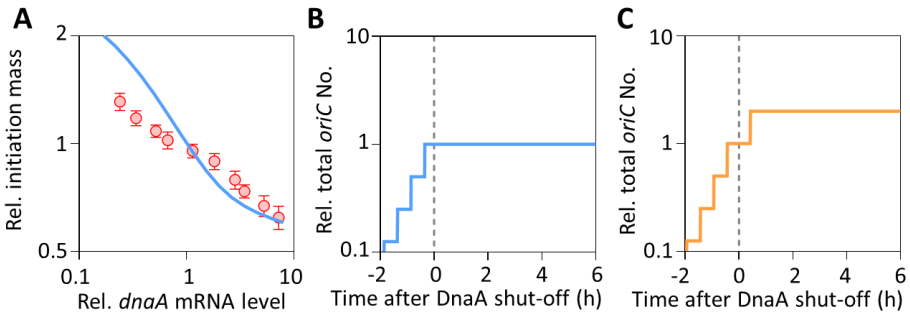

Figure S6. Predictions of the titration-switch model and titration-switch-extrusion model. (A) Comparison of the titration-switch model predictions and experimental data for the relation between relative initiation mass and *dnaA* mRNA levels. The relative initiation mass was calculated as mass/*oriC* averaged over more than 100 cycles after steady DNA replication initiation was established, while the relative *dnaA* mRNA was achieved by setting various *dnaA* expression rate α_A. Dynamics of total *oriC* number during DnaA shut-down predicted by titration-switch model (**B**) and titration-switch-extrusion model (**C**), normalized to the value at DnaA shut-down (dash line).

879 **Table S1. Strains used in this study**

Strain	Relevant genetic marker(s) or features	Source or reference
MG1655	*E.coli K12*(AMB1655)	(Liu et al., 2011)
CL1	MG1655 Δ*cheZ*, Δ*lac*	(Liu et al., 2011)
MGCL1	MG1655 Δ*lac*	This study
RdnaA1	MG1655 P_{dnaA}-*dnaA*::P_{kanR}-*kanR yidA*::(*bla*:P_{tet}-*dnaA*)::*yidX intS*::P_{tet}-*tetR*	This study
RdnaA2	RdnaA1 Δ*lac*	This study
RseqA1	MG1655 *seqA*::*kan attB*::(*bla*:P_{tet}-*tetR-seqA*)	This study
Rhns1	MG1655 *hns*::*kan attB*::(*bla*:P_{tet}-*tetR-hns*)	This study
Rhns2	Rhns1 Δ*lac*	This study
CRidnaA1	MG1655 *asnA::*(P_{J23119}-*sgRNA*$_{dnaA}$*:*P_{J23100}-*tetR:*P_{tet} -*dUn1Cas12f1*)::*viaA*	This study

880

881 **Table S2. Plasmids used in this study**

Plasmid	Relevant genotype	Source or reference
pSIM5	Cm^r , *repA101(Ts) ori,* λRed	(Zheng et al., 2016)
pIkml	Amp^r, pUC *ori*, *loxp-kan-loxp*	(Zheng et al., 2016)
pMD19-tetR	Amp^r, pUC *ori*, *bla:*P_{tet}*-tetR*	(Zheng et al., 2016)
pMD19-hupA-mcherry	Amp^r, pUC *ori*, *bla:*P_{tet}*-tetR-hupA-mcherry*	This study
pMD19-Rhns	Amp^r, pUC *ori*, *bla:*P_{tet}*-tetR-hns*	This study
pMD19-RseqA	Amp^r, pUC *ori*, *bla:*P_{tet}*-tetR-seqA*	This study
pMD19-RdnaA	Amp^r, pUC *ori*, *bla:*P_{tet}*-tetR-dnaA*	This study
p15A-RdnaA	Kan^r, p15A *ori*, P_{tet}*-tetR-dnaA*	This study
pTargetF	*aadA*^{r}, pMB1 *ori*, sgRNA	(Jiang et al., 2015)
pEcCas	Kan^r, pSC101 *ori*, *sacB* P_{araB}-λRed P_{cas}*-cas9*	(Li et al., 2021)
pZA31-P_{tet}-M2-GFP	Cm^r , p15A ori, P_{tet}*-gfp*	(Liu et al., 2019)
CmPcas	Cm^r, pSC101 *ori*, *sacB* P_{araB}-λRed P_{cas}*-cas9*	This study
CPP00458	*aadA*^{r}, pSC101 *ori*, P_{J23119}*-sgRNA-T-*P_{J23100}*-tetR-T-*P_{tet}*-dUn1Cas12f1*	Gift from Fu lab
P_CRidnaA1	*aadA*^{r}, pSC101 *ori*, P_{J23119}*-sgRNA*$_{dnaA}$*-T-*P_{J23100}*-tetR-T-*P_{tet}*-dUn1Cas12f1*	This study
pPT	Cm^r, pSC101 *ori*, BsaI-*lacZa*-BasI-*riboJ-sfgfp*	(Zong et al., 2017)
pPT-RFP	Cm^r, pSC101 *ori*, BsaI-*lacZa*-BasI-*riboJ-mcherry*	This study
pPT-lacZ	Cm^r, pSC101 *ori*, BsaI-*lacZa*-BasI-*riboJ-lacZ*	This study
P_{syn66}-GFP	Cm^r, pSC101 *ori*, P_{syn66}*-riboJ-sfgfp*	This study
P_{con}-GFP	Cm^r, pSC101 *ori*, P_{con}*-riboJ-sfgfp*	This study
P_{syn66}-RFP	Cm^r, pSC101 *ori*, P_{syn66}*-riboJ-mcherry*	This study
P_{native}-GFP	Cm^r, pSC101 *ori*, P_{native}*-riboJ-sfgfp*	This study
P_{syn66}-lacZ	Cm^r, pSC101 *ori*, P_{syn66}*-riboJ-lacZ*	This study
P_{con}-lacZ	Cm^r, pSC101 *ori*, P_{con}*-riboJ-lacZ*	This study
P_{sny66}-P_{con}-FPs	Cm^r, pSC101 *ori*, P_{con}*-riboJ-sfGFP,* P_{syn66}*-riboJ-mcherry*	This study
pET-28a-DnaA	Kan^r, pUC *ori f1 ori*, P_{lacI}*-lacI*, $P_{T7/lacO}$*-dnaA-6*his*	This study
pET-28a-H-NS	Kan^r, pUC *ori f1 ori*, P_{lacI}*-lacI*, $P_{T7/lacO}$*-hns-6*his*	This study

882

883 **Table S3. Primer pairs for synthetic reporter**

Primers	Sequence	Use
DP420 DP421	cctggtagatagattgacaagag*ttatccaca*gtaggatactgagcaca agcttgtgctcagtatcctactgtggataactcttgtcaatctatctac	P_{syn1}
DP422 DP423	cctggtagatagattgacacttgttatacacagggcgatactgagcaca agcttgtgctcagtatcgccctgtgtataacaagtgtcaatctatctac	P_{syn2}
DP424 DP425	cctggtagatagattgacaatac*ttttccaca*ggtagatactgagcaca agcttgtgctcagtatctacctgtggaaaagtattgtcaatctatctac	P_{syn3}
DP426 DP427	cctggtagatagattgacaccgatcattcacagttagatactgagcaca agcttgtgctcagtatctaactgtgaatgatcggtgtcaatctatctac	P_{syn4}
DP428 DP429	cctggtagatagattgacacttgtgtggataagggcgatactgagcaca agcttgtgctcagtatcgccc*ttatccaca*caagtgtcaatctatctac	P_{syn5}
DP430 DP431	cctggtagatagattgaca*ttatccaca*tagttcccgatactgagcaca agcttgtgctcagtatcgggaactatgtggataatgtcaatctatctac	P_{syn6}
DP432 DP433	cctggtagatagattgacacccctgcgat*ttttcccga*tactgagcaca agcttgtgctcagtatcgggaaaaatcgcaggggtgtcaatctatctac	P_{syn7}
DP434 DP435	cctg*ttatccaca*ttgacacccctgcgatagttcccgatactgagcaca agcttgtgctcagtatcgggaactatcgcaggggtgtcaatgtggataa	P_{syn8}
DP436 DP437	cctggtagatagattgacacccctgcgatagttcccgatact*ttatccac* agctgtggataaagtatcgggaactatcgcaggggtgtcaatctatctac	P_{syn9}
DP438 DP439	cctgacagag*ttatccaca*gtagatagattgacaccgatcattcacagttagatactgagcaca agcttgtgctcagtatctaactgtgaatgatcggtgtcaatctatctactgtggataactctgt	P_{syn10}
DP440 DP441	cctggaggggttatacacaactcaaagattgacaccgatcattcacagttagatactgagcaca agcttgtgctcagtatctaactgtgaatgatcggtgtcaatctttgagttgtgtataacccctc	P_{syn11}
DP442 DP443	cctgccatactgtggaaaaggtagaagattgacaccgatcattcacagttagatactgagcaca agcttgtgctcagtatctaactgtgaatgatcggtgtcaatcttctacc*ttttccaca*gtatgg	P_{syn12}
DP444 DP445	cctg*ttatccaca*ttgacacccctgcgatagttcccgatact*ttatccac* agctgtggataaagtatcgggaactatcgcaggggtgtcaatgtggataa	P_{syn13}
DP446 DP447	cctg*ttatccaca*ttgacacccctgcgat*ttttcccga*tactgagcaca agcttgtgctcagtatcgggaaaaatcgcaggggtgtcaatgtggataa	P_{syn14}
DP448 DP449	cctg*ttatccaca*ttgaca*ttatccaca*tagttcccgatactgagcaca agcttgtgctcagtatcgggaactatgtggataatgtcaatgtggataa	P_{syn15}
DP450 DP451	cctggtagatagattgaca*ttatccaca*tagttcccgatact*ttatccac* agctgtggataaagtatcgggaactatgtggataatgtcaatctatctac	P_{syn16}
DP452 DP453	cctggtagatagattgacacccctgcgat*ttttcccga*tact*ttatccac* agctgtggataaagtatcgggaaaaatcgcaggggtgtcaatctatctac	P_{syn17}
DP454 DP455	cctggatagattgacatgtggataagtgtggatgatactgagcaca agcttgtgctcagta*tcatccacacttatccaca*tgtcaatctatc	P_{syn18}
DP456 DP457	cctggatagattgaca*ttatccacagttttcccga*tactgagcaca agcttgtgctcagtatcgggaaaactgtggataatgtcaatctatc	P_{syn19}
DP458 DP459	cctggatagattgaca*ttatccacagctttccaga*tactgagcaca agcttgtgctcagtatctggaaagctgtggataatgtcaatctatc	P_{syn20}
DP460 DP461	cctg*ttatccaca*ttgacacccctgcgatagttcccgatactgtggataa agct*ttatccaca*gtatcgggaactatcgcaggggtgtcaatgtggataa	P_{syn21}
DP462 DP463	cctgtgtggataattgacacccctgcgatagttcccgatact*ttatccac* agctgtggataaagtatcgggaactatcgcaggggtgtcaa*ttatccaca*	P_{syn22}
DP464 DP465	cctgtgtggataattgacacccctgcgatagttcccgatactgtggataa agct*ttatccaca*gtatcgggaactatcgcaggggtgtcaa*ttatccaca*	P_{syn23}
DP466 DP467	cctgtgtggataattgacacccctgcgat*ttttcccga*tactgagcaca agcttgtgctcagtatcgggaaaaatcgcaggggtgtcaa*ttatccaca*	P_{syn24}
DP468 DP469	cctg*ttatccaca*ttgacatgtggataatagttcccgatactgagcaca agcttgtgctcagtatcgggaacta*ttatccaca*tgtcaatgtggataa	P_{syn25}
DP470 DP471	cctgtgtggataattgaca*ttatccaca*tagttcccgatactgagcaca agcttgtgctcagtatcgggaactatgtggataatgtcaa*ttatccaca*	P_{syn26}
DP472 DP473	cctgtgtggataattgacatgtggataatagttcccgatactgagcaca agcttgtgctcagtatcgggaacta*ttatccaca*tgtcaa*ttatccaca*	P_{syn27}
DP474 DP475	cctggtagatagattgaca*ttatccaca*tagttcccgatactgtggataa agct*ttatccaca*gtatcgggaactatgtggataatgtcaatctatctac	P_{syn28}

884

885 **Table S3. Primer pairs for synthetic reporter (continued)**

Primers	Sequence	Use
DP476 DP477	cctggtagatagattgacatgtggataatagttcccgatact*tttatccac* agctgtggataaagtatcgggaacta*ttatccaca*tgtcaatctatctac	P_{syn29}
DP478 DP479	cctggtagatagattgacatgtggataatagttcccgatactgtggataa agct*tttatccaca*gtatcgggaacta*ttatccaca*tgtcaatctatctac	P_{syn30}
DP480 DP481	cctggtagatagattgacacccctgcgatttttcccgatactgtggataa agct*tttatccaca*gtatcgggaaaaatcgcaggggtgtcaatctatctac	P_{syn31}
DP482 DP483	cctggtagatagattgacatgtggataatttttcccgatactgagcaca agcttgtgctcagtatcgggaaaaa*ttatccaca*tgtcaatctatctac	P_{syn32}
DP484 DP485	cctgtgtggataattgaca*ttatccaca*tagttcccgatact*tttatccac* agctgtggataaagtatcgggaactatgtggataatgtcaa*ttatccaca*	P_{syn33}
DP486 DP487	cctg*ttatccaca*ttgaca*ttatccaca*tagttcccgatactgtggataa agct*tttatccaca*gtatcgggaactatgtggataatgtcaatgtggataa	P_{syn34}
DP488 DP489	cctgtgtggataattgaca*ttatccaca*tagttcccgatactgtggataa agct*tttatccaca*gtatcgggaactatgtggataatgtcaa*ttatccaca*	P_{syn35}
DP490 DP491	cctg*ttatccaca*ttgacatgtggataatagttcccgatactgtggataa agct*tttatccaca*gtatcgggaacta*ttatccaca*tgtcaatgtggataa	P_{syn36}
DP492 DP493	cctgtgtggataattgacatgtggataatagttcccgatact*tttatccac* agctgtggataaagtatcgggaacta*ttatccaca*tgtcaa*ttatccaca*	P_{syn37}
DP494 DP495	cctgtgtggataattgacatgtggataatagttcccgatactgtggataa agct*tttatccaca*gtatcgggaacta*ttatccaca*tgtcaa*ttatccaca*	P_{syn38}
DP496 DP497	cctg*ttatccaca*ttgaca*ttatccaca*tagttcccgatact*tttatccac* agctgtggataaagtatcgggaactatgtggataatgtcaatgtggataa	P_{syn39}
DP498 DP499	cctg*ttatccaca*ttgacacccctgcgatttttcccgatact*tttatccac* agctgtggataaagtatcgggaaaaatcgcaggggtgtcaatgtggataa	P_{syn40}
DP500 DP501	cctg*ttatccaca*ttgaca*ttatccaca*gttttcccgatactgagcaca agcttgtgctcagtatcgggaaaactgtggataatgtcaatgtggataa	P_{syn41}
DP502 DP503	cctg*ttatccaca*ttgacaccccc*tttatccaca*cccgatact*tttatccac* agctgtggataaagtatcgggtgtggataaaggggtgtcaatgtggataa	P_{syn42}
DP504 DP505	cctg*ttatccaca*ttgacacccctgcg*ttatccaca*gatact*tttatccac* agctgtggataaagtatctgtggataacgcaggggtgtcaatgtggataa	P_{syn43}
DP506 DP507	cctg*ttatccaca*ttgacatgtggataatagttcccgatact*tttatccac* agctgtggataaagtatcgggaacta*ttatccaca*tgtcaatgtggataa	P_{syn44}
DP508 DP509	cctg*ttatccaca*ttgacaccccttgtggataacccgatact*tttatccac* agctgtggataaagtatcggg*ttatccaca*aggggtgtcaatgtggataa	P_{syn45}
DP510 DP511	cctg*ttatccaca*ttgacaccccctgcgtgtggataagatact*tttatccac* agctgtggataaagtatc*ttatccaca*cgcaggggtgtcaatgtggataa	P_{syn46}
DP512 DP513	cctg*ttatccaca*ttgacattttcccgatagttcccgatact*tttatccac* agctgtggataaagtatcgggaactatcgggaaaatgtcaatgtggataa	P_{syn47}
DP514 DP515	cctg*ttatccaca*ttgacatcgggaaaatagttcccgatact*tttatccac* agctgtggataaagtatcgggaactattttcccgatgtcaatgtggataa	P_{syn48}
DP516 DP517	cctg*ttatccaca*ttgacaccccttttcccgacccgatact*tttatccac* agctgtggataaagtatcgggtcgggaaaaaggggtgtcaatgtggataa	P_{syn49}
DP518 DP519	cctg*ttatccaca*ttgacaccccttcgggaaaacccgatact*tttatccac* agctgtggataaagtatcgggttttcccgaaggggtgtcaatgtggataa	P_{syn50}
DP520 DP521	cctg*ttatccaca*ttgacacccctgcgtcgggaaaagatact*tttatccac* agctgtggataaagtatcttttcccgacgcaggggtgtcaatgtggataa	P_{syn51}
DP522 DP523	cctgtgtggataagatagattgacatgtggataagtgtggatgatactgagcaca agcttgtgctcagta*tcatccacacttatccaca*tgtcaatctatc*ttatccaca*	P_{syn52}
DP524 DP525	cctg*ttatccaca*gatagattgaca*ttatccaca*gctttccagatactgagcaca agcttgtgctcagtatctggaaagctgtggataatgtcaatctatctgtggataa	P_{syn53}
DP526 DP527	cctg*ttatccaca*gatagattgaca*ttatccaca*gttttcccgatactgagcaca agcttgtgctcagtatcgggaaaactgtggataatgtcaatctatctgtggataa	P_{syn54}
DP528 DP529	cctg*ttatccaca*gatagattgacatgtggataagtgtggatgatactgagcaca agcttgtgctcagta*tcatccacacttatccaca*tgtcaatctatctgtggataa	P_{syn55}
DP530 DP531	cctgtgtggataattgacatgtggataagtgtggatgatactgagcaca agcttgtgctcagta*tcatccacacttatccaca*tgtcaa*ttatccaca*	P_{syn56}

886

887 **Table S3. Primer pairs for synthetic reporter (continued)**

Primers	Sequence	Use
DP532 DP533	cctgttgacattatccacagttttcccgatactttatccac agctgtggataaagtatcgggaaaactgtggataatgtcaa	P_{syn57}
DP534 DP535	cctgttatccacattgacatgtggataatttttcccgatactttatccac agctgtggataaagtatcgggaaaaattatccacatgtcaatgtggataa	P_{syn58}
DP536 DP537	cctgttatccacattgacattatccacatttttcccgatactgtggataa agctttatccacagtatcgggaaaaatgtggataatgtcaatgtggataa	P_{syn59}
DP538 DP539	cctgtgtggataattgacattatccacatttttcccgatactttatccac agctgtggataaagtatcgggaaaaatgtggataatgtcaattatccaca	P_{syn60}
DP540 DP541	cctgtgtggataattgacattatccacatttttcccgatactgtggataa agctttatccacagtatcgggaaaaatgtggataatgtcaattatccaca	P_{syn61}
DP542 DP543	cctgtgtggataattgacatgtggataatttttcccgatactttatccac agctgtggataaagtatcgggaaaaattatccacatgtcaattatccaca	P_{syn62}
DP544 DP545	cctgttatccacattgacatgtggataatttttcccgatactgtggataa agctttatccacagtatcgggaaaaattatccacatgtcaatgtggataa	P_{syn63}
DP546 DP547	cctgtgtggataattgacatgtggataatttttcccgatactgtggataa agctttatccacagtatcgggaaaaattatccacatgtcaattatccaca	P_{syn64}
DP548 DP549	cctgtgtggataattgacatgtggataagtgtggatgatacttgtggata agcttatccacaagtatcatccacacttatccacatgtcaattatccaca	P_{syn65}
DP550 DP551	cctgttatccacattgacattatccacagttttcccgatactttatccac agctgtggataaagtatcgggaaaactgtggataatgtcaatgtggataa	P_{syn66}
DP552 DP553	cctgtgtggataattgacatgtggataagtgtggatgatactttatccac agctgtggataaagtatcatccacacttatccacatgtcaattatccaca	P_{syn67}
DP554 DP555	cctgttgacacccctgcgatagttcccgatactgagcaca agcttgtgctcagtatcgggaactatcgcaggggtgtcaa	P_{con}
DP556 DP557	cctgttatccacacccgggttatccacagttttcccgagcccttatccac agctgtggataagggctcgggaaaactgtggataacccgggtgtggataa	P_{neg}

888

889

890 **Table S4. Oligonucleotides for the construction of strains and plasmids**

Primers	Sequence	Use
DJP001	gaaagaggagaaatactagatgaccatgattacggattcac	Amplifying *lacZ* gene *from* MG1655 genome
DJP002	ttgatgcctggcttatcattatttttgacaccagaccaact	
DJP003	gaaagaggagaaatactagatggtttccaagggcgagg	Amplifying mCherry gene *from* pMD19-*hupA-mcherry*
DJP004	ttgatgcctggcttatcattatttgtagagctcatccatgc	
DJP005	ccacaaggtctccagctgatcaagatcctgcaaaacgat	Amplifying native *dnaA* promoter (P_{native}) *from* MG1655 genome
DJP006	ccacatggtctcccctgccaatttttgtctatggtcat	
DJP007	ctgttttcttgcaagattactagtccatccagtgctcatttgtacagttcatccatacc	Amplifying P_{con}-*gfp* cassette *from* P_{con}-GFP plasmid
DJP008	ccttagtgactcctgcagtcctgggtgttgacacccctgcgat	
DJP009	cgccatatgtcactttcgctttggca	Amplify *dnaA* gene *from* MG1655 genome for the construction of pET-28a-DnaA plasmid
DJP010	cgcaagcttttacgatgacaatgttctga	
DJP011	cgccatatgagcgaagcacttaaaat	Amplify *hns* gene *from* MG1655 genome for the construction of pET-28a-H-NS plasmid
DJP012	cgcaagcttttattgcttgatcaggaaatc	
DJP013	cgatctgcagaaagaggagaaatactaggtgtcactttcgctttggc	Amplifying *dnaA* gene *from* MG1655 genome
DJP014	gtgagccggatccttacgatgacaatgttctgatt	
DJP015	atgcctgcagtcacacaggaaacctactagatgaaaacgattgaagttgatgatg	Amplifying *seqA* gene *from* MG1655 genome
DJP016	gtcaggatccttagatagttccgcaaaccttct	
DJP017	cagtaagcttaaagaggagaaatactagatgagcgaagcacttaaaattc	Amplifying *hns* gene *from* MG1655 genome
DJP018	gtacggatccttattgcttgatcaggaaatcgtcg	
DJP019	tggatcgcgaagaaaggc	Amplifying T3-P_{tet}-*tetR-dnaA* cassette *from* pMD19-RdnaA *plasmid*
DJP020	tcgatatcaaccatggctgcggcaaaatcgctcgagt	
DJP021	cgttttatttgatgggtcgacctgcagggaaagccacgt	Amplifying *kanr* gene from the plasmid pEcCas
DJP022	ttcttcgcgatccatgctagcagcaaccaattaaccaattc	
DJP023	gcagccatggttgatatcgagctcgcttgga	Amplifying p15A-T_1 fragment from the PZA31-P_{tet}-M2-GFP plasmid
DJP024	cacatgaagtcgacccatcaaataaaacgaaaggctc	
DJP025	tcaacccactgcagcaaccaattaaccaattctgattacgccccgccctgcca	Amplifying Cm^r gene from pZA31-P_{tet}-M2-GFP plasmid for the construction of CmPcas
DJP026	tgtctgcttacataaacagtaatacaaggggtgttatggagaaaaaaatcactgg	
DJP027	ttaaaggtattaaaaacaacttttttgtctttttaccttcccgtttcgctccaggaaacagctat gaccatg	Amplifying the T_0-Amp-T_1-P_{tet}-*tetR-hns* or T_0-Amp-T_1-P_{tet} -*tetR-seqA cassette,* and then assembling to *attB* locus via *λRed* recombination system
DJP028	cacaggttgctccgggctatgaaatagaaaaatgaatccgttgaagcctgtgtaaaacga cggccagt	
DJP029	tctattattacctcaacaaaccaccccaatataagtttgagattactacaatgattgaacaa gatggattgcac	Amplifying kan^r gene from plkml plasmid for the deletion of native *hns* gene
DJP030	aaaaaatcccgccgctggcgggattttaagcaagtgcaatctacaaaagatcagaagaa ctcgtcaagaagg	
DJP031	ggcctgcacgattgtggattgccattgctttgtcctttgtctgcaacgttctagtgaacctctt cgaggg	Amplifying kan^r gene from plkml plasmid for the deletion of native *seqA* gene
DJP032	catatactcctggcgacttgtattcagctaagacactgcactggattaaggccgatcatatt caataaccc	
DJP033	gagtcatgcacagattcgta	*T0-*P_{tet}*-tetR-T3* cassette was amplified from plasmid *pMD19-tetR with primers DJP035/DJP036, the intS upstream and downstream sequences were amplified from MG1655 genome with primers DJP033/DJP034, and DJP037/DJP038, respectively. Three fragments were ligated via overlap PCR with primers DJP033/DJP038.*
DJP034	gatctgaagcgaaccatga	
DJP035	tcatggttcgcttcagatcaggttgtgtgttcctcttcattc	
DJP036	cctcatagccgatttgtttgaaggaaacagctatgaccatga	
DJP037	caaacaaatcggctatgagg	
DJP038	agtgtataagggtgttcagc	
DJP039	gtacgttagatcgtagacgcttggcgataaagaacgccacttcgcccggccgtgagcattt aggatccggctcaccttca	Amplifying T3-kanr-T1 cassette from p15A-RdnaA plasmid to replace the native P_{native}-*dnaA* on the genome
DJP040	gatcgattaagccaatttttgtctatggtcattaaattttccaatatgcggcgtaaatctagg gcggcggatttg	
DJP041	ttaggcaccccaggctttac	The *dnaA*-T_3 and T_0-Amp-T_1-P_{tet} fragments were amplified from the pMD19-RdnaA plasmid using primers DJP041/DJP042 and DJP043/DJP044, respectively. These two fragments were then combined via overlap PCR using primers DJP045/ DJP046 to generate a homologous recombination fragment for inserting T_0-Amp -T_1-P_{tet}-*dnaA*-T_3 between the *yidA* and *yidX* genes.
DJP042	cagtgatagagatactgagcacataagcttaaagaggagaaagactaggtgtcactttcgc	
DJP043	gtgctcagtatctctatcactgatagggatgtcaatctctatcactgatagggagggactcgag	
DJP044	aaaacgacggccagtgaa	
DJP045	gatggcgtggcgtttgctattgagaagtatgtgctgaattaatctgtgggcggtcatcttcggctactgtct	
DJP046	accgctgcaatttctggttgtatatgcagtaaaccaataatcagtaagcgcaggaaacagctatgaccatg	
DJP047	saacttcgagtggagtccgccgtg	Inserting to the CPP00458 backbone to generate P_CRidnaA1 plasmid to shut down *dnaA* expression
DJP048	cgagcacggcggactccactcgaa	

891
892

893 **Table S4. Oligonucleotides for the construction of strains and plasmids (continued)**

Primers	Sequence	Use
DJP049 DJP050	aaacgatgaagaccgtctttctcc ttcttagacgtcaggtggcattattacagcagagaagggacg	Amplifying homologous sequences to *asnA* gene
DJP051 DJP052	tgccacctgacgtctaagaa tctagattactgcgcagatggcgacgataatgacagcagccaactcagcttc	Amplifying P_{J23119}-*sgRNA*$_{dnaA}$:P_{J23100}-*tetR*:P_{tet}-*dUn1Cas12f1* cassette from P_CRidnaA1 plasmid
DJP053 DJP054	gccatctgcgcagtaatctagatcgcatcccggtatcaaagc atgaacagtgtgcgaaagcg	Amplifying homologous sequences to *viaA* gene
DJP055 DJP056	ccacaaggcatcgaacaagc gtggaacccggtactggaag	Assembling the upper three fragments through overlap PCR
DJP057 DJP058	cttctttggtgctgtactca tggttgatatcgagcaagtg	RT-qPCR primer for *rpoA*
DJP059 DJP060	cccgattgcaggatgagtt tacccaatcgaggacaaaac	RT-qPCR primer for *dnaA*
DJP061 DJP062	cgttatccggaccatatgaa cttcaaatttcacttccgca	RT-qPCR primer for *gfp*
DJP063 DJP064	aagttaaactgcgtggtact acaggtttcttggctttgta	RT-qPCR primer for *mcherry*
DJP065 DJP066	tatgttgaaattttccgccg attcatccgaaagcagaagt	RT-qPCR primer for *seqA*
DJP067 DJP068	gtattgacccgaacgaactg agtccaggttttagtttcgc	RT-qPCR primer for *hns*

894

895

896

897

898 **Table S5. 43 3'-TAMRA probes spanning the whole coding sequence of the *dnaA* gene**

gccaaagcgaaagtgacacg	agaacgataggtcggttctg	cttcctgagatcgttcttta	cacgaagtcgatggtgatcg
tgcaatcgggcaagacactg	acgtgtgtttgacgtttacg	ggcgttgaaggtgtggaaaa	tgaccagtttttcctgcaat
aattctgtggctggtaactc	cgccagttggttagatttac	atctgttgattaccttccag	ccgtcttctgaatattgtcg
caatgggcgtatccacatac	ggaacaacgggttataggca	atagcgatccgaggtgagaa	cgcgactttgatcttgtagt
agcgtgttatcgctcagttc	atgcagcaggtgagttttac	caacgccgttgatctctttc	atcgacgcttggaaaggaga
cccaatcgaggacaaaacgg	taaaccactttggcattcgg	caaccgaagcgggatttcaa	tgtggttagtcagctctttc
ttattaaggtacttgtcccg	tgaacaaagcgctcggagtg	tttttcatcaggatcgccac	caccaaacgcatcgccaatc
gcagaaactggttagcagtc	tttgcagggctttaaccatg	acgaatgtcgttttcgtcgg	ttacggcaggcatgaagcac
cgacttcaaaacgcagctgt	ttaaactcttcgatcgcgtt	ggcgataaagaacgccactt	ctcttcacgcaactgctcga
gtagaaggcgcagcacgttg	atctacggaacggtagtagc	gtacgttagatcgtagacgc	aatcttctttgatatcgtgg
ggacgttatcccaacctgag	gaatatcgtcgatcagcagt	ggtaaagttggcattggcaa	

899

900

Table S6. Parameters used in models

Parameter	Description	Values	Source
	Titration model & Extrusion model		
λ	Biomass growth rate	$1.54h^{-1}$	This study (if not specifically defined)
α_A	DnaA synthesis rate	$300\ h^{-1}\mu m^{-3}$	Fitted in this study
$[A_f^c]$	Threshold of DnaA concentration	$10\ \mu m^{-3}$	Fitted in this study
α_H	Extruder synthesis rate	$180\ h^{-1}\mu m^{-3}$	Fitted in this study
η	Relative noise level of λ and α_A in stochastic model	0.1	*Fitted in this study*
	Switch model		
$[D]_T$	Concentration of total DnaA protein	$400\mu m^{-3}$	(Berger & Wolde, 2022) SI table 2 LDDR model
α_l	Activation rate of DnaA-ATP by lipid	$750h^{-1}$	
α_{d1}	Activation rate of DnaA-ATP by the *DARS1* site	$100h^{-1}$	
α_{d2}	Activation rate of DnaA-ATP by the *DARS2* site	$643h^{-1}$	
β_{datA}	Deactivation rate of DnaA-ATP by *data* site	$600h^{-1}$	
β_{rida}	Deactivation rate of DnaA-ATP by RIDA system	$500h^{-1}$	
K_D	Dissociation constant of DnaA activation and deactivation	$50\mu m^{-3}$	
K_D^P	Dissociation constant of DnaA promoter	$300\mu m^{-3}$	
f_C	Threshold of DnaA-ATP fraction for DNA replication initiation	0.75	
	Titration switch model & Titration-switch-extrusion model		
K_D^P	Dissociation constant of DnaA promoter	$400\mu m^{-3}$	(Berger & Wolde, 2022) SI table switch-titration model
n	Cooperativity of dnaA expression	5	
α_H	Extruder synthesis rate	$550\ h^{-1}\mu m^{-3}$	Fitted in this study
$[A_{ATP}^{fc}]$	Threshold of DnaA-ATP concentration for DNA replication initiation	$200\mu m^{-3}$	Fitted in this study

Note S1

To understand the initiation mass dependency on *dnaA* expression level α_A (Fig. 2G), we can solve the dynamics of DnaA amounts $A_{(t)}$ and cell volume $V_{(t)}$, yielding the solutions: $A_{(t)} = \frac{\alpha_A V_0}{\lambda} e^{\lambda t} + const$. The boundary conditions corresponding to successive rounds of DNA replication initiation at times $t = 0$ and $t = t_I$ are: $A_{(t=0)} = \frac{A_I \cdot O}{2} + \frac{A_b}{2}$, $V_{(t=0)} = \frac{V_I \cdot O}{2}$, and $A_{(t=t_I)} = A_I \cdot O + A_b$, $V_{(t=t_I)} = V_I \cdot O$, where A_I is the threshold of DnaA number per *oriC* and V_I is the cell volume per *oriC* at the time of initiation (t_I).

Applying these conditions, we derive

$$V_I = \frac{A_I - A_b}{\alpha_A} \lambda$$

showing that the initiation mass is inversely proportional to the DnaA expression level α_A, assuming A_I and A_b are constant. This inverse relationship predicted by the titration model implies a much sharper dependence of initiation mass on DnaA expression than the exponential dependence observed experimentally.

Following the same analysis in the titration model, the extrusion model has the same DnaA amounts and volume dynamics as in the titration model with similar H-NS dynamics $H_{(t)} = \frac{\alpha_H V_0}{\lambda} e^{\lambda t} + const$. The condition of DNA replication initiation sets the boundary condition:$A_{(t=0)} = \frac{A_I \cdot O}{2} + \frac{A_b}{2} + H_{(t=0)}$, $V_{(t=0)} = \frac{V_I \cdot O}{2}$ and $A_{(t=t_I)} = A_I \cdot O + A_b + H_{(t=t_I)}$, $V_{(t=t_I)} = V_I \cdot O$.

Solving these equations we get:

$$V_I = \frac{A_I - A_b}{\alpha_A + \alpha_H} \lambda$$

The adding of extruder shifts the inverse dependency of initiation mass - dnaA expression curve to the left which results in a flatter curve. To get a better fitting to experiment data, $\alpha_H = 1500\ h^{-1} \mu m^{-3}$ were used in Fig. 6G.